Lateral Ag Electrodeposits in Chalcogenide Glass for Physical Unclonable Function Application

by

Ninad Chamele

A Thesis Presented in Partial Fulfilment
of the Requirements for the Degree
Master of Science

Approved April 2017 by the
Graduate Supervisory Committee:

Michael Kozicki, Co-Chair
Hugh Barnaby, Co-Chair
Nathan Newman

ARIZONA STATE UNIVERSITY

May 2017

ABSTRACT

Counterfeiting of goods is a widespread epidemic that is affecting the world economy. The conventional labeling techniques are proving inadequate to thwart determined counterfeiters equipped with sophisticated technologies. There is a growing need of a secure labeling that is easy to manufacture and analyze but extremely difficult to copy. Programmable metallization cell technology operates on a principle of controllable reduction of a metal ions to an electrodeposit in a solid electrolyte by application of bias. The nature of metallic electrodeposit is unique for each instance of growth, moreover it has a treelike, bifurcating fractal structure with high information capacity. These qualities of the electrodeposit can be exploited to use it as a physical unclonable function. The secure labels made from the electrodeposits grown in radial structure can provide enhanced authentication and protection from counterfeiting and tampering.

So far only microscale radial structures and electrodeposits have been fabricated which limits their use to labeling only high value items due to high cost associated with their fabrication and analysis. Therefore, there is a need for a simple recipe for fabrication of macroscale structure that does not need sophisticated lithography tools and cleanroom environment. Moreover, the growth kinetics and material characteristics of such macroscale electrodeposits need to be investigated. In this thesis, a recipe for fabrication of centimeter scale radial structure for growing Ag electrodeposits using simple fabrication techniques was proposed. Fractal analysis of an electrodeposit suggested information capacity of 1.27×10^{19}. The kinetics of growth were investigated by electrical

characterization of the full cell and only solid electrolyte at different temperatures. It was found that mass transport of ions is the rate limiting process in the growth. Materials and optical characterization techniques revealed that the subtle relief like structure and consequently distinct optical response of the electrodeposit provides an added layer of security. Thus, the enormous information capacity, ease of fabrication and simplicity of analysis make macroscale fractal electrodeposits grown in radial programmable metallization cells excellent candidates for application as physical unclonable functions.

To my grandparents

ACKNOWLEDGMENTS

I would like to express my deepest gratitude to my advisors Dr. Michael Kozicki and Dr. Hugh Barnaby for their support of my research. I thank Dr. Kozicki for his invaluable guidance and mentorship. Dr. Kozicki's energy and resourcefulness has been my inspiration throughout this work. I would also like to thank Dr. Barnaby for his constant encouragement and great patience with me. I'm amazed by all the efforts and time he puts in for the success of his students.

I would like to thank my committee member Dr. Nathan Newman for letting me use his labs and training me on the instruments. I'm grateful to Dr. Newman for always been enthusiastic about my research and never failing to provide new ideas to explore.

I am indebted to Dr. Yago Gonzalez Velo who has supported and advised me throughout my research career at ASU. I am grateful for Jennifer Taggart, Wenhao Chen and Adnan Mahmood for always helping me when I needed help. I would like to thank Mehmet Balaban for providing the AFM analysis of my samples. I would also like to thank my colleagues Hemanth Kumar Balaji, Arshey Patadia, Anand Krishnan and Runchen Fang who have supported my research and enabled completion of this work.

I want to thank all my friends who have been a major part of my life and who motivated me throughout my career. Lastly, I would like to thank my sister and my parents, without their love I would not be here.

TABLE OF CONTENTS

Page

CHAPTER Page

LIST OF TABLES

LIST OF FIGURES

Figure Page

1 INTRODUCTION

1.1 Motivation

Counterfeit goods are inferior goods that are made and sold under a brand's name without their permission. Counterfeiting not only violates the patents, trademarks or copyrights of the manufacturer but also weakens trust of the consumer in the brand owing to inferior quality of counterfeit goods. Counterfeit goods are deliberately made such that their appearance is similar to their genuine counterparts in order to mislead the customer. Therefore, spotting and getting rid of counterfeit goods can be extremely difficult. Counterfeiting has infiltrated virtually every segment of products such as food, clothes, automobiles, jewelry, electronics etc.; but it has more serious implications when the counterfeit goods compromise safety and security of individuals. Especially in high reliability, high stake sectors such as defense, aerospace, automotive, and healthcare, counterfeiting of goods may lead to loss of vital resources or even worse, life. There exist some anticounterfeiting measures that employ tags such as watermarking, holograms, and barcodes for labeling products. However, they all can be compromised by a determined counterfeiter.

Programmable metallization cell (PMC) technology is mainly famous for its nonvolatile memory version [1], popularly known as conductive-bridging random access memory (CBRAM[*]). However, the technology has many applications that arise from its unique operating principle. PMCs function by controllable growth of a metallic

[*] CBRAM is registered trademark of Adesto Technologies Corporation

electrodeposit with electrical stimulus. The metallic electrodeposits have an intricate branching fractal structure that has a unique set of details for every instance of formation. The random and unique nature of these electrodeposits make them an excellent candidate for physical unclonable function (PUF) [2]. A PUF is a physical entity that is very easy to observe but extremely difficult to predict or replicate. Labels can be created out of these electrodeposits that are grown radially using typical materials used in PMC technology. The labels could be overtly or covertly attached to an item and serve as a unique signature of the item thus protecting it against counterfeiting. The geometrical details of these electrodeposits can be converted to a large random integer by using appropriate algorithms that would be associated with the item. Scanning of the label would yield a number that could be matched against a global database of items to determine its authenticity. Tampering with the label would either change the output random number or would not result in a number at all thereby indicating an instance of tampering upon which fate of the item may be decided as desirable. The random number obtained from the electrodeposits can also be used for other security applications such as session authentication, keys for secure encryption etc. Thus, given their high complexity and inherent uniqueness, tags made of electrodeposits grown using PMC technology offer superior protection against counterfeiting and tampering compared to conventional secure labeling techniques.

So far only microscale electrodeposits have been fabricated and investigated [3]. Radial PMCs for microscale electrodeposits need to be fabricated in a cleanroom environment with advanced lithography techniques, moreover, the need for sophisticated imaging instruments for their scanning and analysis limits their application to only high value

products. Therefore, there is a need for establishing a fabrication recipe for radial PMCs that can grow electrodeposits on a macroscale and have minimum number of simple fabrication steps in order to widen the applicability of these labels. Electrodeposits have been successfully grown in radial PMCs in previous works but little is known about the underlying processes and growth kinetics, especially for large electrodeposits. This thesis aims to address these issues by developing a recipe for fabrication of centimeter scale radial PMCs for growth of macro electrodeposits, investigating their growth kinetics and further characterizing them using various materials and optical characterization techniques.

1.2 Thesis outline

This thesis will explore electrodeposits grown in radial PMCs for application as PUFs. Chapter 2 of this thesis provides a brief overview of various types of PMCs and their applications. Chapter 3 discusses the materials for PMCs, the underlying processes that govern their operation and the laws that control these processes. Chapter 4 explores the fractal properties of electrodeposits grown in PMCs along with an evaluation of information capacity of an electrodeposit grown radially. Chapter 5 presents the fabrication methods used for making centimeter scale radial PMCs in this work and their characterization using different electrical, materials and optical analysis techniques. Chapter 6 summarizes the work and offers a conclusion.

2 PROGRAMMABLE METALLIZATION CELL TECHNOLOGY

The PMC technology encompasses the family of devices that leverages electrochemical reduction of an active metal between two electrodes [4]. A PMC is simply an electrochemical cell consisting of an active anode and an inert cathode separated by a solid electrolyte with active metal dissolved in it. The PMC technology has many applications such as nonvolatile memory [1], timers [5], RF switches [6], and microfluidic valves [7]. The broad functionality of the PMC can be attributed to the change in its electronic, optical or structural properties as a result of controlled reduction of metal cations into a metallic electrodeposit. In a typical PMC, the active metal anode serves as a source of metal ions and the inert electrode acts as a counter electrode. When the cell is energized by applying a potential to the anode, it oxidizes and gives up cations of the active metal. The cations travel through the solid electrolyte under the electric field established by the applied potential and get reduced at the cathode forming metallic electrodeposit on the cathode. This electrodeposit can subsequently be grown by continuing to apply the bias or be dissolved back in the electrolyte by applying reverse bias.

A PMC can be fabricated into different geometries depending on the desired application. Three important geometries namely vertical, lateral and radial are discussed below.

2.1 Vertical PMCs

Undoubtedly the most widely known variant of PMC due to its application as a nonvolatile memory device, vertical PMCs have gained immense popularity in the semiconductor industry recently. They are often hailed as replacement of NAND flash as

storage class memory because of their low power, nonvolatile and fast switching properties. The vertical PMC has many monikers, CBRAM, electrochemical memory (ECM), cation migration based memory, nanoionic memory to name a few [8]. CBRAM is a type of resistance change memory (RRAM) that stores information as a function of resistance of the memory cell. A representative structure of CBRAM is shown in Fig. 1.

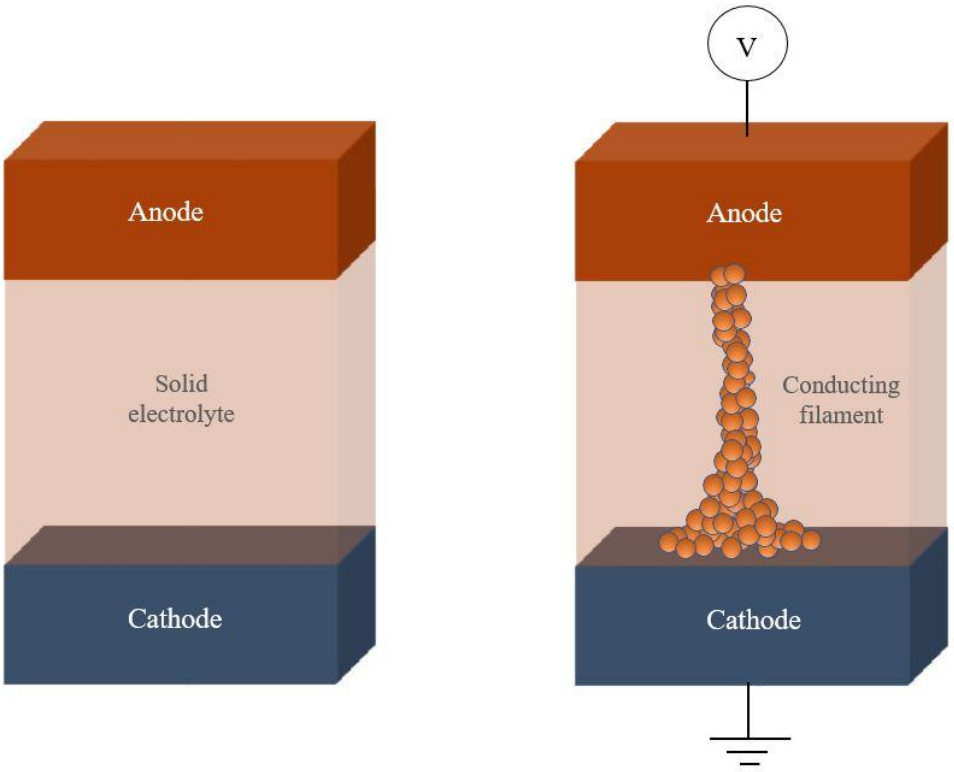

(a) (b)

Figure 1:Vertical PMC in high resistance (a) and low resistance state (b)

As can be seen from the figure, the solid electrolyte is sandwiched between top active anode and bottom inert cathode [1]. The fabrication of CBRAM involves a dedicated processing step for dissolution of active metal into the solid electrolyte depending on the material system. The thickness of the solid electrolyte usually ranges from a few

nanometers to tens of nanometers. When positive bias is applied on the anode with respect to cathode, the anode oxidizes to give metal ions as,

$$M = M^{+} + e^{-}. \quad (1)$$

The M^{+} ions drift towards the bottom cathode under the field and get reduced at the cathode by gaining an electron and subsequently grow into a metallic filament. The reduction reaction is given as,

$$M^{+} + e^{-} = M. \quad (2)$$

The metallic filament shorts the two electrodes and switches the resistance of cell from high resistance state to low resistance state. On application of reverse bias, a combination of negative applied potential and joule heating from high currents through the metallic filament causes it to oxidize and dissolve back into the solid electrolyte. The dissolution of the filament increases the resistance between the electrodes and the cell switches back to high resistance state. Information is stored in CBRAM in the form of resistance. The filament is retained when the bias is removed because of its metallic nature, so the stored information in the memory is not destroyed even after power to the device is turned off, granting it low power and nonvolatile qualities. The electric fields in vertical PMCs can be enormous owing to the smaller nanoscale thickness of the solid electrolyte. Due to the planar nature of the device, electric field vectors are lined up mostly uniformly between the electrodes and thus the metallic filaments are highly directional. Moreover, the filament thickness can only reach few nanometers since the device itself is very thin.

2.2 Lateral PMCs

Unlike vertical PMCs where the solid electrolyte is sandwiched vertically between the electrodes in a metal-electrolyte-metal stack, lateral PMCs have electrodes on top of the electrolyte film, which is doped with the active metal. Moreover, the distance between the electrodes is usually a few microns compared to a few nanometers in vertical PMCs. An advantage of the lateral geometry and greater electrode spacing is that the metallic electrodeposit can be observed visually. The electric fields in lateral PMCs are smaller as compared to vertical PMCs but are still measurable; therefore, the electrodeposit is still highly directional but is generally thicker. The electrodeposit can grow either on the surface or beneath it. A typical structure is shown in Fig. 2.

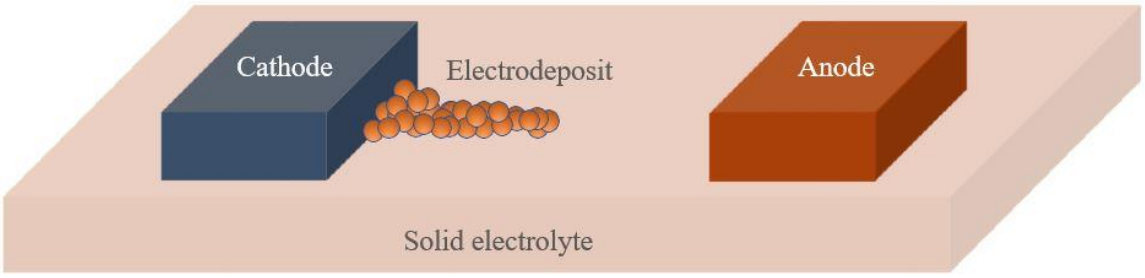

Figure 2: Lateral PMC

The operation of the cell is similar to that of vertical PMCs. The metallic electrodeposit can be grown or retracted by application of positive or negative bias to the anode. Lateral PMCs can have many applications for the same planar geometry of the cell or a slight modification of it. Some of the applications of lateral PMCs are discussed below.

2.2.1 Radio Frequency (RF) switches

RF switches are used to route high frequency signals through transmission routes. Conventional microelectromechanical systems (MEMS) devices are used as RF switches e.g., cantilever MEMS switch, fixed-fixed MEMS switch etc. MEMS devices are extremely complicated to fabricate and need a constant power supply to operate. Lateral PMCs are excellent replacements of MEMS devices as RF switches owing to their nonvolatile nature and ease of fabrication. The switch turns on when the electrodeposit shorts the two electrodes and turns off when the electrical contact is broken [6]. The ON state resistance of the PMC depends on thickness of the metallic electrodeposit which can be controlled by increasing the amount of current through the cell and in turn depositing more active metal. Therefore, a very small ON state resistance for the switch is possible. The small ON state resistance allows for smaller insertion loss caused by the insertion of a lossy device in the transmission line.

2.2.2 Microfluidic valve

The lab-on-chip technology is a family of microanalytical devices that combines multiple laboratory processes on a single integrated circuit. The advantages of these devices are reduction in consumption of chemicals, ability to work with extremely small sample volumes, shorter analysis times and reduction in costs. Realization of these devices relies on the ability to precisely control and manipulate analyte fluids. Microfluidic valves allow electrical control of flow through microchannels. A schematic of lateral PMC used as a microfluidic valve is shown in Fig.3.

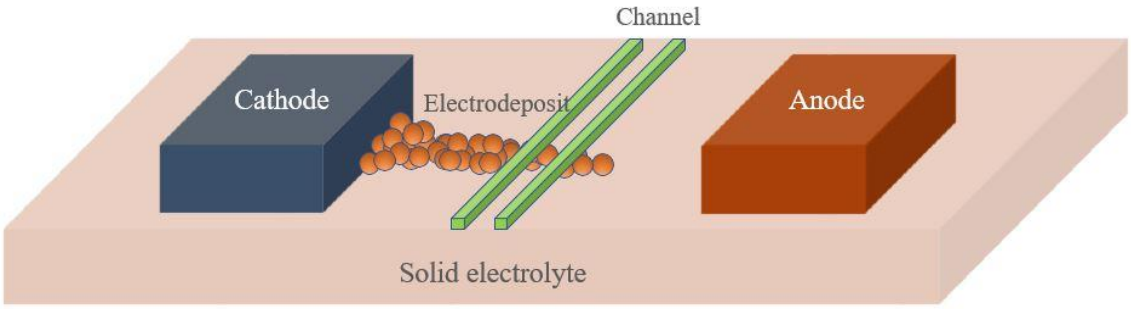

Figure 3: Lateral PMC as microfluidic valve

The electrolyte channel of the PMC is fabricated at right angles to the direction of flow to be controlled [7]. The valve is turned off by growing the metallic electrodeposit in the channel by application of bias to the anode. The high surface area metallic structure of the electrodeposit changes the fluid-surface interaction in the channel and increases the contact angle for water by at least 20°, hence stopping the fluid flow. The analyte flow can be resumed by reversing the bias on the anode. The combination of negative applied potential and joule heating in the filament causes the metallic electrodeposit blocking the flow to retract, switching the valve off. Thus, the hydrophobic nature of the channel can be controlled electrically.

2.2.3 Timers

Lateral PMCs can be used as timers by electrically characterizing the growth of metallic electrodeposit with time [5]. A Timer application of a lateral PMCs hinges on the property of the metallic electrodeposit to grow only when the cell is biased. Conventional solid state timers such as solid state relays do not retain their state during loss of power while the nonvolatile nature of lateral PMCs allows them to retain the time information even in the absence of power. Fig. 4 illustrates use of lateral PMCs as timer devices. The structure of

lateral PMCs as a timer deviates from the usual two electrode geometry of conventional PMCs. A third ‘sensing’ electrode is incorporated in the design to gauge the change in electrical properties of the cell as shown in Fig. 4. The device is biased periodically to grow the electrodeposit. The change in length of the electrodeposit changes the impedance of the structure as measured by the sensing electrode. Since the growth rate of the electrodeposit is controlled by the amount of charge passing through the anode, the change in impedance can be calibrated to measure the amount of time that has passed.

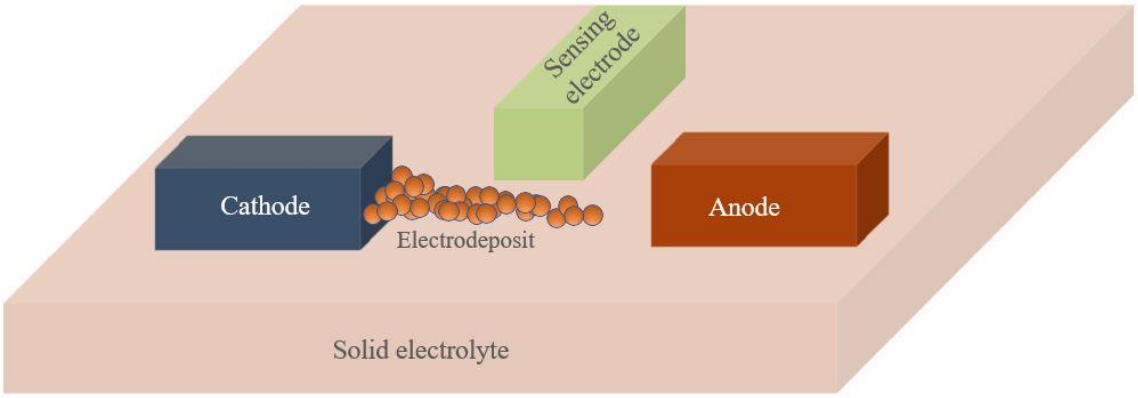

Figure 4: Lateral PMC as a timer device

The change in electrical properties are measured between the sensing electrode and the inert cathode since the growth of the electrodeposit starts at the cathode. The timer device has applications from high stake defense electronics to consumer electronics. Since the device is nonvolatile, it can be used as a runtime monitor to measure the time the circuit has been on.

2.3 Radial PMCs

Radial PMCs are similar to their vertical and lateral cousins in that they operate on the same principal of growing a metallic electrodeposit between two electrodes in a solid state electrochemical cell and that is where the similarities end. An illustrative structure of a radial PMC is shown in Fig.5. Radial PMCs have a planar geometry, the active anode has a circular shape, cathode being a small point at the center of that circle. The solid electrolyte encompasses the area of the circle and serves as the channel region where the metallic electrolyte is grown. The implication of having a circular anode and a cathode at its center is that when the device is biased, the electric field at every point in the device points towards the focal cathode; unlike vertical or lateral PMCs where the field is unidirectional at each point in the channel. The magnitude of the initial electric field in radial PMCs depends on the radius of the anodic circle. Radial PMCs can be fabricated with anode radius of few micrometers to a few centimeters. The concentric nature of isoelectric field lines along the circumference of anode ensures that there is equal chance that the electrodeposit will grow in any direction. Therefore, on application of positive potential to the anode, the electrodeposit grows in a random pattern.

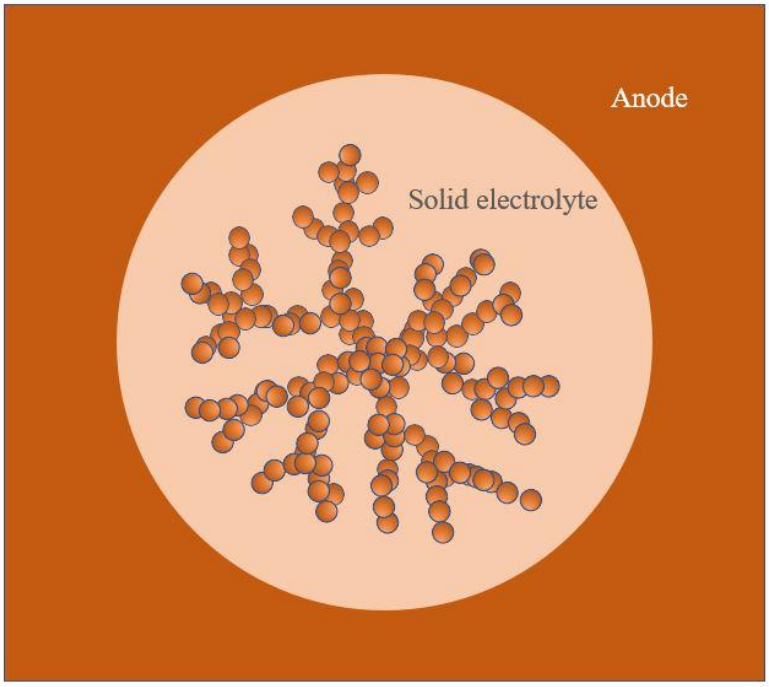

Figure 5: Radial PMC with metallic electrodeposit

The randomness of the electrodeposits grown in radial PMCs can be leveraged to use them as a PUF [2]. Later chapters will discuss how electrodeposits in radial PMCs can be used as PUFs. The application of radial PMCs as a PUF is inherently different than other applications discussed so far because it is mainly based on appearance and therefore the optical properties of the electrodeposits as opposed to their electrical properties in the case of vertical and lateral PMCs. In this work, we investigate the electrodeposits in radial PMCs for their application as PUFs, particularly their electrical, materials and optical characterization and underlying principles of their growth.

3 MATERIALS, PHYSICS AND CHEMISTRY OF RADIAL PMCs

3.1 Materials

The majority of the research pertaining to materials systems in PMCs have been focused on vertical PMCs on account of their use as nonvolatile memory application. A wide range of materials ranging from oxides, chalcogenides, halides and even insulating polymers have been used as solid electrolytes [9]. The seemingly diverse bulk properties of these materials tend to converge at nanoscopic scales of thickness in vertical PMCs resulting in similar electrolytic and ionic conduction properties [10]. Mobility of active ion in the solid electrolyte is the most important property that governs switching characteristics in CBRAM. The small thickness of electrolyte and consequently extremely high fields associated with vertical PMCs ensure that even slower ion conductor systems display resistive switching at adequate speeds. The radial PMCs however deal with larger fields of solid electrolytes between electrodes compared to vertical PMCs. As a result, the choice of materials system narrows down only to the active metal-solid electrolyte pairs that show fast ion conduction at room temperature. Moreover, the same materials should also exhibit superior thermal stability owing to the high temperature processing steps such as thermal evaporation and annealing.

In solid electrolytes, after the active metal atom is ionized, the conduction of ions takes place by random thermally activated hopping within the matrix. The mobility of ions depends on the size of ions; smaller ions can move between the sites in the material readily and have higher mobility. The ease of reversible redox reaction of the active metal depends on how reactive it is. Elements with smaller ionic radius such as sodium (Na) and potassium

(K) have extremely high mobilities but are also extremely reactive making their reduction back to pure, metallic form energetically very expensive. Moreover, such metals are also very unstable during processing and have lower electrical conductivity. From this point of view, silver (Ag) and copper (Cu) are ideal choices for active metal. They have high mobilities, can be easily oxidized or reduced electrochemically and have excellent electrical conductivities in their metallic form. Most importantly, they form superionic binary phases with chalcogens such as sulfur (S), selenium (Se) and tellurium (Te); these binary phases have extremely high ionic mobility and can withstand higher temperature. However, their properties are highly sensitive to composition and temperature and hence they cannot be used directly as solid electrolytes in PMCs [11]. This problem can be solved by forming a ternary phase of active metal, chalcogen and germanium (Ge). Chalcogens form glassy alloys with germanium (Ge) that can withstand high temperature processing and have insulating properties. This glassy host matrix can be made to dissolve the active metal by means of irradiation with ionizing radiation such as UV light, gamma rays etc., a phenomenon also known as photodissolution or photodoping [12]. The result is a ternary that has a form of robust, continuous, and glassy Ge rich backbone which has in it a uniformly dispersed nanoscale active metal-chalcogenide superionic binary phase. The active metal rich binary phase has high ionic and electronic conductivity while the backbone Ge rich matrix is an insulator which governs the resistivity of the solid electrolyte. It should be noted that for the active metal to successfully dissolve and form the superionic binary phase with chalcogen the glassy Ge-chalcogenide matrix should have excess chalcogen content than the stoichiometric composition. The cathode may be chosen from any of the relatively inert metals such as Ni, W, Pt etc. [8], it can either be fabricated

separately on the structure or can be a part of the instrument setup used for biasing the cell. The cathode only serves the purpose of connecting the electrochemical cell and providing counter charge.

In this work, Ag was selected as an active material and a Ge-Se glassy matrix was selected as the backbone structure. Ag was chosen instead of Cu owing to its higher nobility to prevent oxidation of the electrodeposit on exposure to ambient. Se was chosen instead of S as a chalcogen to form binary phase with Ag; this was because the binary Ag_2Se has higher ionic mobility than Ag_2S which means it would take shorter time to grow an electrodeposit of Ag in a selenide system compared to a sulfide system. This was particularly important since the radial PMCs fabricated in this work had radius of 1.5 cm which is extremely large compared to lateral or vertical PMCs. The ratio of Ge to Se in the glassy matrix was chosen to be 30 to70. $Ge_{30}Se_{70}$ has slightly more Se concentration than the stoichiometric $GeSe_2$ which aids the dissolution of Ag as discussed. The 30 to 70 ratio was selected owing to the optimum mobility and stability of this composition.

3.2 Basic processes in radial PMCs

The ability to redistribute mass is where all the attractive applications of PMCs stem from and electrochemical reactions in the cell make this possible. The processes involved in redistribution of mass in PMC can be divided into three steps, oxidation of Ag anode to Ag^+ ions, transport of these ions through the solid electrolyte and subsequent reduction of these ions at the cathode back to metallic Ag. These processes are discussed in this section.

3.2.1 Electrochemical reactions

In view of how vital the electrochemical reactions are to the PMC, it befits one to understand them in detail. For sake of simplicity, we consider at a simple metal-electrolyte-metal PMC as shown in Fig.6.

Figure 6: Ag-chalcogenide-W PMC

The $Ge_{30}Se_{70}$ chalcogenide is doped with Ag and acts as a solid electrolyte. Since the Ag anode is more reactive metal than tungsten (W) cathode, it has more tendency to undergo oxidation as,

$$Ag \rightarrow Ag^{+} + e^{-}. \qquad 3$$

Under equilibrium conditions when the cell is formed and there is no applied bias, the Ag^{+} ion concentration in the solid electrolyte in the immediate vicinity of the Ag anode has a strong consequence on its energy or potential level and hence on its tendency to lose an electron. As the amount of Ag^{+} in the solid electrolyte decreases, the Ag anode metal

becomes more active and as a result has more negative energy. It will dissolve or oxidize readily because it would have much greater tendency to dissolve into an uncrowded electrolyte. The Nernst equation can be used to calculate energy or potential E of Ag anode in the solid electrolyte with a known quantity of Ag^+ ions [13]. It can also be used to calculate the change in the potential when the concentration of the Ag^+ ions in the solid electrolyte changes. It is given as,

$$E = E_0 + \frac{RT}{nF} \ln\ [Ag^+], \qquad 4$$

where

E_0 = Energy level or potential of Ag under standard conditions,

R = Universal gas constant,

T = Temperature,

n = Number of electrons released per atom oxidized,

F = Faraday's constant, and

$[Ag^+]$ = concentration of Ag^+ in the solid electrolyte.

Similarly, the potential of W cathode can also be calculated and hence the potential of the full cell is obtained by subtracting individual electrode potentials. The Nernst equation describes the cell voltage at equilibrium condition which is analogous to leaving the fabricated PMC unbiased and measuring the potential across the cathode and the anode. At equilibrium, the net current through the device is zero. However, that does not mean that there are no ongoing redox reactions in the PMC. The nature of the equilibrium in such cells is dynamic. The Ag oxidation at anode and its reverse reaction of reduction at cathode continues without application of bias but the rate of these reactions is equal. Therefore, the currents associated with cathodic and anodic reactions are equal and opposite but zero in

total. The cathodic or anodic current at equilibrium is also referred to as exchange current i_o. It should be noted that there are two types of currents in an electrochemical cell depending on where they originate from. The originating from redox reactions at the electrode-electrolyte interfaces are called faradaic currents and the currents originating from the movement of ions are called non-faradaic currents.

To grow an electrodeposit in PMCs, they need to be biased to speed up the redox reactions at the electrode surfaces. At such non-equilibrium conditions, the reaction kinetics are described by Butler-Volmer equation [13]. The equation describes how the electrical current density j through an electrode depends on its potential. It is given as,

$$j = j_o.\left\{exp\left[\frac{\alpha_a nF}{RT}\left(E - E_{eq}\right)\right] - exp\left[-\frac{\alpha_c nF}{RT}\left(E - E_{eq}\right)\right]\right\}, \quad 5$$

where

j_0 = Exchange current density,

E = Applied electrode potential,

E_{eq} = Potential under equilibrium conditions,

R = Universal gas constant,

T = Temperature,

n = Number of electrons released per atom oxidized,

α_c = Cathodic charge transfer coefficient ($1 \geq \alpha_c \geq 0$),

α_a = Anodic charge transfer coefficient ($1- \alpha_c$) and

F = Faraday's constant.

The Butler-Volmer equation gives the maximum current possible at given applied voltage on the electrodes for specified conditions. This equation is valid when the rate limiting process is governed by charge transfer at the electrode interface for redox reactions.

However, if the rate limiting process in PMC is mass transport from the anode to cathode, the current is controlled by the transport properties of the electrolyte.

3.2.2 Transport of ions

The electrochemical reactions only take place at the electrode-electrolyte interfaces. It is the transport properties of the solid electrolyte that govern the movement of ions from anode to cathode and vice versa. Moreover, the volume covered by the solid electrolyte is enormous compared to the electrode-electrolyte interfaces. Therefore, it is vital to describe transport of ions through the solid electrolyte to understand kinetics of the cell. It is well known that ion conduction in solid electrolytes is accomplished by ionic hopping. In case of Ag in Ag doped Ge-Se chalcogenide, the ionic transport takes place through electric field driven, thermally activated Mott-Gurney correlated hopping [14]. According to Mott-Gurney model, the mobile Ag^+ ions in doped Ge-Se chalcogenide reside in potential wells separated by small barriers and the ions can readily hop from one position to next. The hopping process is characterized by thermionic emission over an energy barrier between adjacent sites. The hopping current density j_{hop} is given by,

$$j_{hop} = ZqN_i a\nu \exp\left(-\frac{W}{kT}\right)\sinh\left(\frac{aZq\varepsilon}{2kT}\right), \qquad 6$$

where

a = Mean ionic hopping distance,

ν = Hopping frequency,

Zq = Charge on the cation,

N_i = Cation concentration,

T = Temperature (K),

K = Boltzmann constant,

W = Height of energy barrier and

ε = Applied electric field.

In the absence of electric field, all the barriers are of the same height in all directions, therefore there is equal probability of the ion to jump into any of the potential wells around it. However, on application of electric field, the barrier lowers along the direction of the applied field and the probability of ion hopping in that direction increases, thus increasing the current in that direction. Both the cases are shown in Fig.7.

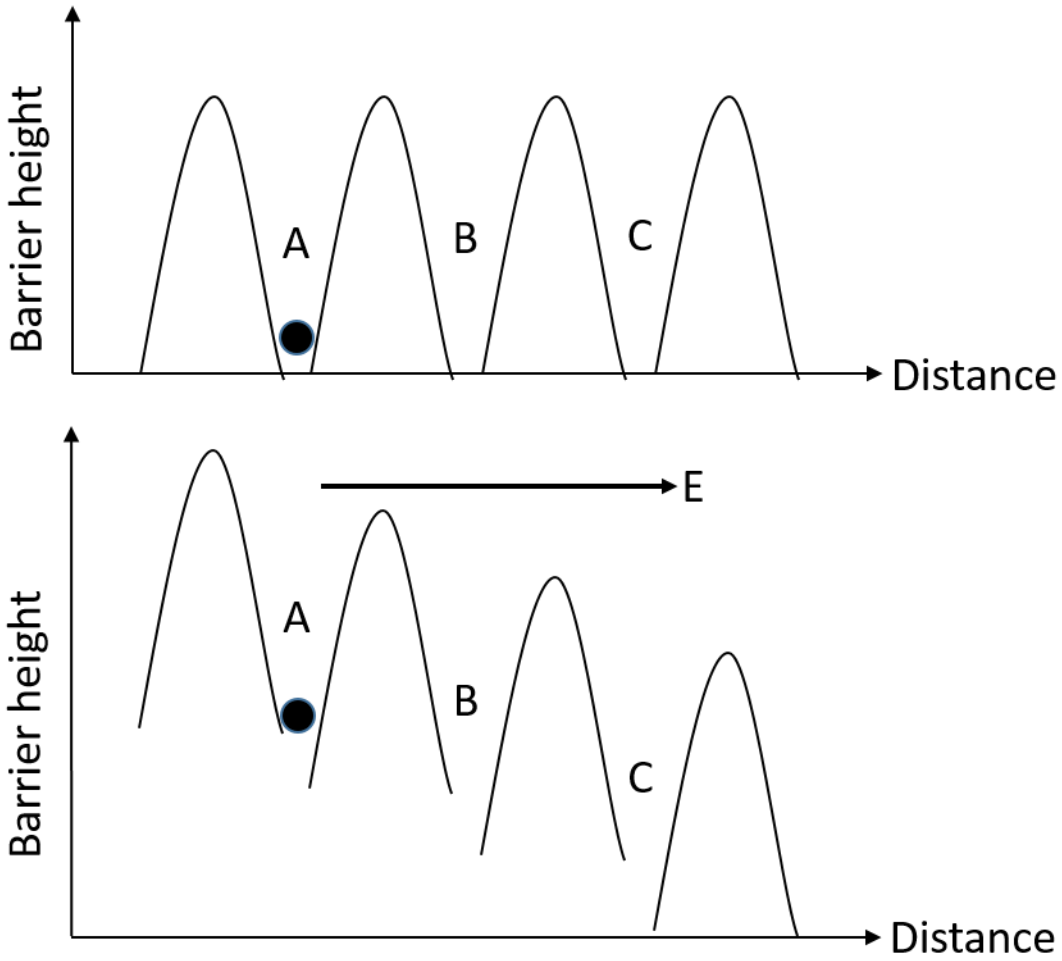

Figure 7: Barrier lowering in Mott-Gurney hopping

At high electric fields, Eq. 6 reduces to

$$j_{hop} = ZqN_i a\nu \exp\left(-\frac{W}{kT}\right)\exp\left(\frac{aZq\varepsilon}{2kT}\right). \quad 7$$

Therefore, the I-V curve shows exponential behavior for high fields in Mott-Gurney hopping conduction. At low fields, Eq. 6 reduces to a linear form showing linear I-V behavior as

$$j_{hop} = \frac{(Zq)^2 N_i a^2 \nu\varepsilon}{kT}\exp\left(-\frac{W}{kT}\right). \quad 8$$

4 PHYSICAL UNCLONABLE FUNCTIONS AND FRACTALS

4.1 Electrodeposits as physical unclonable functions

The electrodeposits grown in radial PMCs have intricate branching structure which is self-similar when viewed at different scales. Moreover, although the electrodeposits look 2-dimensional to the naked eye, they possess 3-dimensional microscale surface morphology that grants them unique optical properties. Their fractal nature and therefore high information capacity can be utilized to generate secret keys that can be used to produce a challenge response pair which have a number of security applications such as session authentication, secure keys for encryption or even as secure anticounterfeit package labels. Especially in their application as secure labels, their unique surface morphology provides an added layer of protection against tampering and counterfeiting as will be discussed in later chapters.

For security applications, such as the ones mentioned above, physical unclonable functions are used to generate a unique number because, as the name suggests, they are extremely difficult to copy. Apart from being able to provide a large number of unique random numbers, the key requirements of a physical unclonable function are that they [15]:

- should be simple to evaluate but extremely hard to predict
- should be easy to fabricate but practically impossible to duplicate even if their exact manufacturing process is known
- should preserve the information it represents in case of noise.

In view of these requirements, a function based on random processes in nature appears to be an obvious choice for a PUF as long as the process is truly random and scalable. It has been established that the randomness in the electrodeposits in radial PMCs originates from the stochastic nature of diffusion of ions. The process by which the irregular fractal like pattern of the electrodeposit is created is called diffusion limited aggregation [16] [17]. The fractal nature of these patterns originates from the entropy provided by diffusion process [18]. Even if the geometry of electrodeposit is random due to mass transport properties of ions, its growth is still controllable owing to the energetic barrier for the redox reaction. The electrodeposit can only be grown when the cell is biased and is provided sufficient energy to overcome activation energy of the redox reaction and series resistance of the electrolyte. When the cell is biased, Ag^+ ions in the solid electrolyte start nucleating at the cathode. The moment an ion in the vicinity of cathode undergoes reduction by gaining an electron from cathode, it becomes immobile Ag. The immobile Ag now becomes a part of the cathode and acts a source of electrons for other Ag^+ ions to get reduced at. It is important to note that the reduction of Ag^+ ion will create a concentration gradient in the uniformly doped solid electrolyte. Moreover, since the immobile Ag has essentially changed the shape of cathode, the concentric isoelectric field lines in the cell at the beginning would change from circular to irregular depending on its new shape. Therefore, ions move towards the cathode by drift-diffusion under the new concentration gradient and electric field. The growth of electrodeposit now proceeds outward while being supplied by random hopping motion of ions under constantly changing electric field and concentration gradient. The presence of field means there is some directionality to the motion of ions. However, the fields in radial PMCs are not substantial. Moreover, the

presence of electric field only influences the hopping of ions in its direction, the ionic motion perpendicular to the field is still unaffected. The initial nucleation of Ag at the cathode is an important step in dictating the shape of the electrodeposit since the electrodeposit grows in a preferential direction owing to high fields from shortened distance between the cathode and itself. Moreover, the reduction of ions and consequent growth of the electrodeposit depletes the concentration of Ag^+ ions in the area around it. The combination of increasing electric field and competition for ions between two growing fronts of electrodeposits culminates in branchlike form with bifurcations throughout the pattern, with limited range of angles between and no crossing between two branches. An implication of the electrodeposit growth being controllable by turning the power on or off is, the size of the electrodeposit can be controlled. The size of the electrodeposit can range over several orders of magnitude depending on the size of the cell and how long they have been biased. At the same time, the electrodeposits retain their fractal nature and high information entropy and therefore their trustworthiness as PUFs, as will be seen in the upcoming sections. Therefore, the electrodeposits can be used at different sizes of labels for different applications from covert tagging at microscale to big boxes and enclosure.

4.2 Information in fractal structures

A fractal is a geometric pattern that repeats itself at different scales [19]. Fractals look the same irrespective of the scale, even an extremely small part of the shape looks the same as the entire shape, a property also known as self-similarity. A fractal can be created by starting with a simple pattern and repeating it at smaller scales infinitely. Of course, practically it is impossible to create a perfect fractal because of the atomic size limit;

nevertheless, approximate fractal shapes can be constructed and their properties studied. Fig. 8 shows one of the most famous fractals, a Koch curve [20]. The Koch curve is constructed by starting with a line segment as shown. The line segment is then divided into three equal segments and an equilateral triangle that has the middle segment as base and is pointing outward is drawn. Removing the line segment that is the base of the triangle gives the next generation of the fractal as shown in the figure. Iteratively altering each line segment infinitely as described above gives a Koch curve. The Fig. 8 shows 6 generations of the Koch curve. Fractals are characterized by fractional numbers as their dimensions. Whenever a D dimensional object is scaled by a factor S, its constituents (length in 1 dimension, area in 2 dimensions) change by a factor of S^D. This is because the object scales by a factor of S in D dimensions. The dimension of fractal objects is called Hausdorff or fractal dimension and is given by

$$D = \frac{\log N}{\log S}, \tag{9}$$

where, N is number of elemental pieces that make up the full object and S is the scaling factor, the ratio by which the full object is bigger than the elemental piece. In the case of Koch curve, since there are 4 sides to the curve in generation 1 and each side is 3 times smaller than the original segment, N is 4 and S is 3, which gives fractal dimension of (log 4)/(log 3) = 1.26186. It can be seen from the figure that N increases as scaling factor S increases with generation for example, in the Koch curve, the value of N increases from 4 to 16 to 64 for increase from 3 to 9 to 27 of the scaling factor from generation 1 to 2 to 3.

Therefore, using Eq. 9, if a fractal can be resolved to the n^{th} generation, the number of elements N_n that can be observed is given by,

$$N_n = S_n^D \qquad 10$$

where S_n is scale factor at generation n.

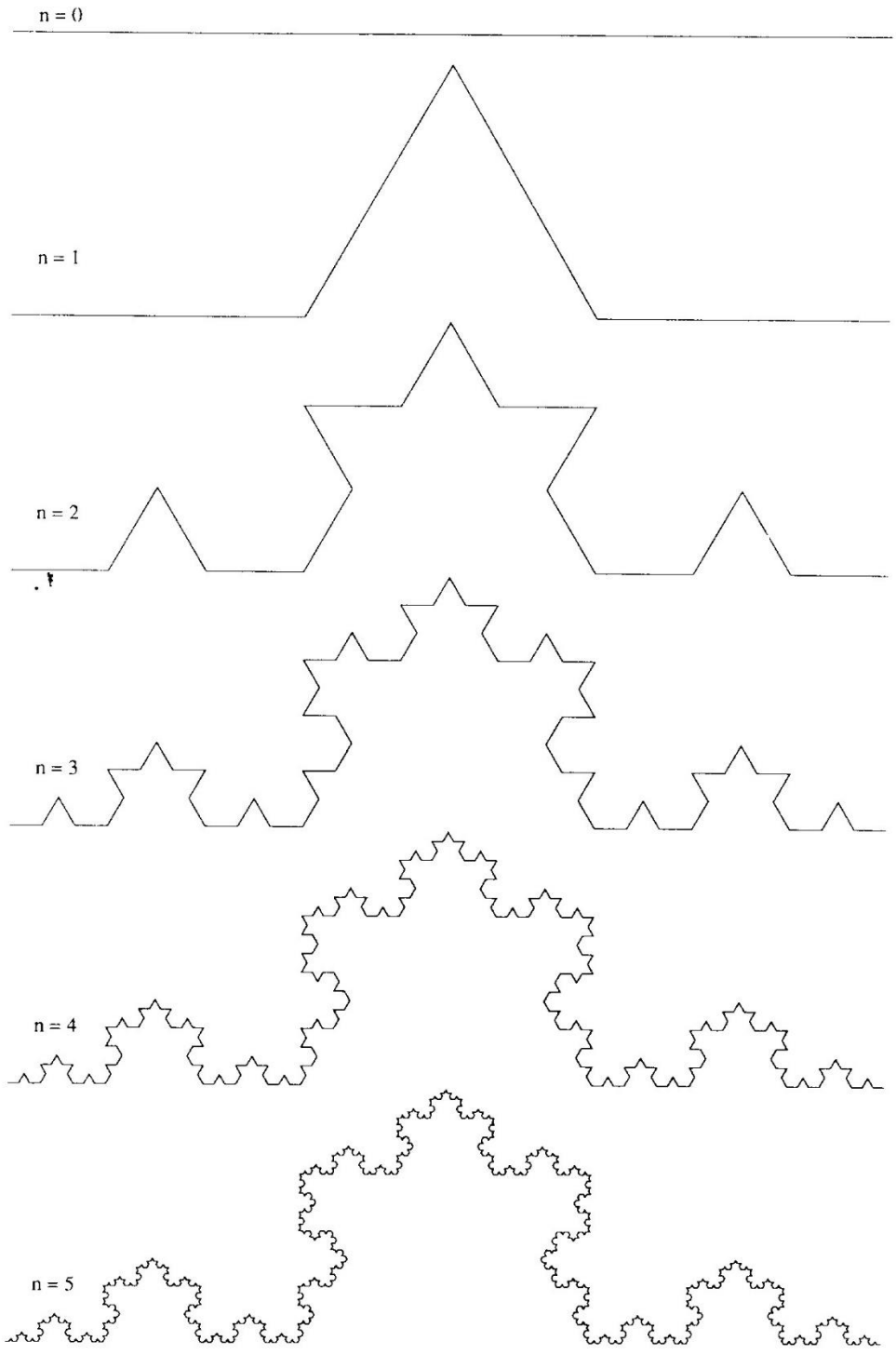

Figure 8: Six generations of the Koch curve

Clearly the number of self-similar units increases as the generation of fractal increases. Each self-similar unit in the fractal object can be used to represent information if it is modified in a way to allow determination of its state later. For example, in case of Koch curve in generation 1, the color of middle two segments at 60° to each other could be changed to red from black to represent 1 and no color change would mean 0. Higher order representation is also possible by using different schemes for coding. The number of self-similar units that can be used to encode information in fractals depends on the magnification used to image the fractal, higher the magnification more the number of self-similar units that can be resolved. For every generation of the fractal n, the number of information units is given by,

$$\mu_n = \frac{N_1^n}{N_1} = N_1^{n-1}, \tag{11}$$

where, N_1 is the number of elements in first generation shape. N_1 is related to initial scale S_1 by,

$$N_1 = S_1^D. \tag{12}$$

Therefore,

$$\mu_n = S_1^{D(n-1)}. \tag{13}$$

If a magnification factor M at generation n is defined as

$$M = \frac{S_n}{S_1} = \frac{S_1^n}{S_1} = S_1^{n-1}. \tag{14}$$

Then by substituting value of M in Eq. 13, we get a relationship between number of readable units μ_n, magnification factor M and fractal dimension D as,

$$\mu_n = M^D. \quad 15$$

The number of unique instances or information capacity I_n that is possible at n_{th} generation fractal depends on the coding scheme that has been used to encode information in the single readable unit. For a coding scheme that can represent information in B states in a single element, the information capacity is given by,

$$I_n = B^{\mu_n} = B^{M^D}. \quad 16$$

Information capacity increases as a double exponential function. Therefore, the fractals allow a huge number of unique complex patterns to be encoded in them which can be decoded to give large integers that can be used as secret keys in variety of applications as discussed above.

4.3 Information in fractal electrodeposits

Figure 9: Bright-field photomicrograph of fractal Ag electrodeposit

Fig. 9 shows photomicrograph of a fractal Ag electrodeposit grown in a radial PMC taken at 100x. Although the electrodeposit is not a perfect fractal with regular self-similar arrangement of identical elemental pieces, it still has self-similar scaled properties that are repeated.

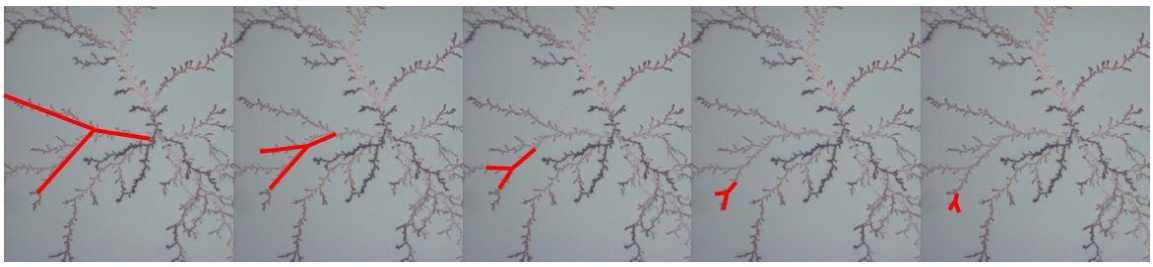

Figure 10: Five generations of self-similar Y-shaped elements in fractal Ag electrodeposit

For example, the bifurcating branches of the electrodeposit making a Y-shape can be seen at different scales, as shown in Fig. 10. Because of the irregular nature of this fractal, the bottom up approach of finding the fractal dimension as described in the earlier section cannot be used here. Therefore, box counting method was used for calculation of fractal dimension. In box counting method, squares of a given size S are used to cover the image of electrodeposit and the minimum number of squares N required to cover the image are counted.

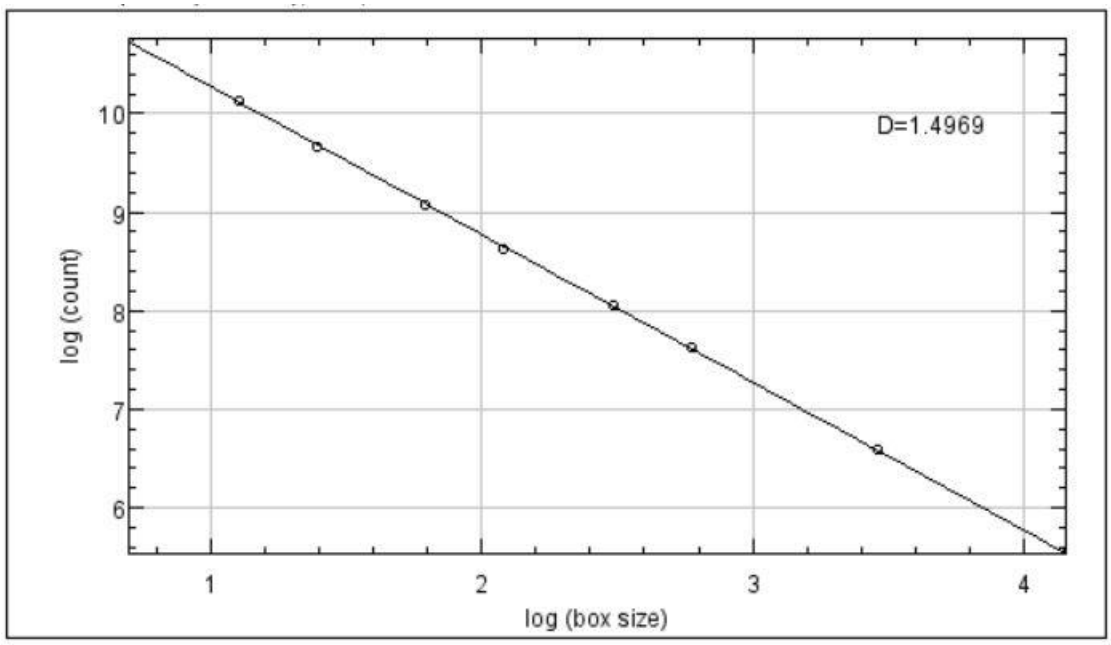

Figure 11: Calculation of fractal dimension by using box counting method

The same procedure is repeated at different sizes of squares to arrive at a plot of log N vs log S as shown in Fig. 11. The slope of the curve is the fractal dimension D given by, D = log N/log S. The box counting method was used to find the fractal dimension of electrodeposit shown in Fig. 9, the analysis was performed using ImageJ software. The calculated fractal dimension of the electrodeposit is 1.497. The information capacity of the electrodeposit shown in Fig. 9 can be calculated using the method discussed in earlier section. Fig. 10 shows 5 generations of Y-shaped branches that can be resolved in the photomicrograph, the length of each branch being approximately half the size of the branch in previous generation. Therefore, in our case n = 5, and S1 = 2 since the length of a branch in second generation is approximately 2 times smaller than the length of the branch in first generation. Therefore, by using Eq. 14, we find M = 16. The information can be encoded in these electrodeposits by considering a single Y-shaped bifurcation as an information unit. The schemes could use variety of the electrodeposit characteristics as a parameter that determines the state of the data for example, length of the branches, the angle between them etc. If a simple binary scheme is assumed (B = 2), the information capacity of the given pattern is,

$$I_n = B^{M^D} = 2^{16^{1.497}} = 1.27\times10^{19}. \quad 17$$

5 DEVICE FABRICATION AND CHARACTERIZATION

5.1 Fabrication of radial PMCs and growth of electrodeposit

The radial PMCs are easy to fabricate with only four processing steps and no need of optical lithography techniques owing to their simple structure and large size. The radial PMCs investigated in this work were fabricated at Nanoionic Prototyping Facility in Center for Applied Nanoionics at Arizona State University. The fabrication steps were as follows:

5.1.1 Wafer preparation and isolation layer

Even though the electrodeposit can be grown on rough surfaces, a silicon (Si) wafer was chosen as a substrate instead to be able to easily characterize the grown electrodeposit with various materials characterization techniques. The Si wafers were RCA cleaned and a protective photoresist layer was spun on the surface after, followed by dicing into 2 cm x 2 cm squares. The squares so obtained were then cleaned with AZ 400T stripper at 130 °C and washed with water. A 200 nm isolation layer of SiO_2 was then deposited on the substrates with Plasma Enhanced Chemical Vapor Deposition (PECVD) technique in Oxford PECVD as shown in Fig. 12.

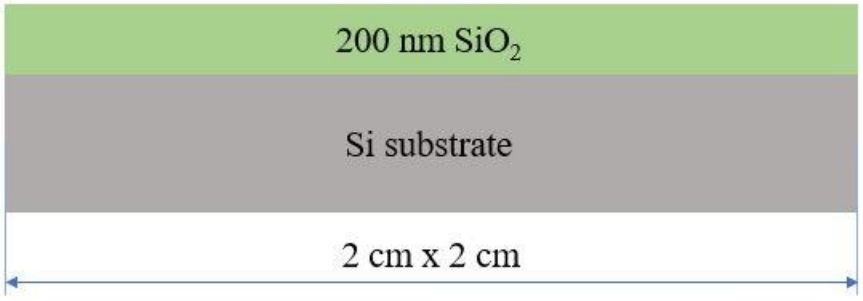

Figure 12: Deposition of SiO_2 isolation layer with PECVD

5.1.2 Deposition of Ag anode

A 60 nm thick circular Ag anode was then deposited around the circular channel area by using a metal template of 1.5 cm diameter as a shadow mask. The deposition was done in a Cressington 308R thermal evaporation system. The chamber vacuum for deposition was better than $1x10^{-6}$ mbar. The evaporation of Ag was carried out by heating the boat containing Ag thermally at 4 V operating voltage and 45 A deposition current. The deposition rate was about 0.1 nm s^{-1} as monitored by crystal thickness monitor.

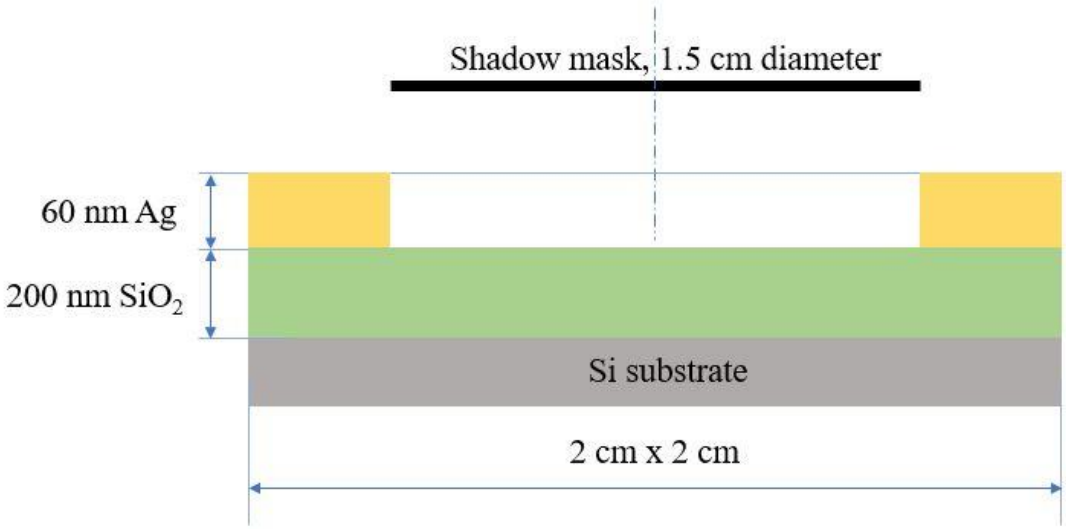

Figure 13: Deposition of Ag anode by using a circular shadow mask

5.1.3 Deposition of $Ge_{30}Se_{70}$ and photodoping Ag

After the Ag anode deposition, the vacuum was broken and the shadow mask was removed. The samples were then placed back again in the Cressington 308R system for further processing. An 80 nm thick blanket film of $Ge_{30}Se_{70}$ was then deposited on the Ag anode with thermal deposition as shown in Fig. 14. The chamber vacuum for deposition was better than $1x10^{-6}$ mbar, evaporation of $Ge_{30}Se_{70}$ was done by heating another boat containing a glassy $Ge_{30}Se_{70}$ precursor thermally at 4 V operating voltage and 35 A deposition current. The deposition rate was about 0.1 nm s^{-1} as monitored by crystal thickness monitor. Followed by the deposition of $Ge_{30}Se_{70}$, a 20 nm Ag blanket film which serves as a source of Ag for photodissolution in $Ge_{30}Se_{70}$, was deposited without breaking the vacuum. The deposition conditions for Ag were same as the ones for the Ag anode.

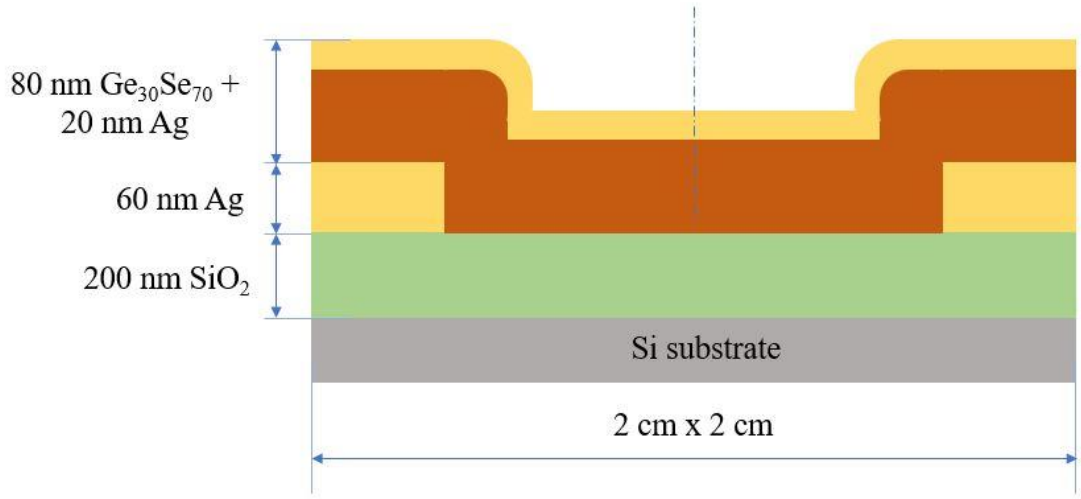

Figure 14: Deposition of $Ge_{30}Se_{70}$ and Ag for photodissolution

5.1.4 Photodissolution of Ag with ultraviolet (UV) light

The samples so prepared were irradiated with UV light for 2 hr to bring about photodissolution of Ag into the chalcogenide film. The UV light drives the Ag into $Ge_{30}Se_{70}$ which subsequently reacts with excess selenium to form nanoclusters of Ag_2Se in the Ge rich backbone structure forming a solid electrolyte as shown in Fig. 15. The UV light was UVA with 3.4 eV energy and the source had intensity of 3.5 m W cm^{-2}. Fig. 16 shows top and side view schematics of the device after fabrication is complete. These devices were then biased to form Ag electrodeposits in the radial PMC.

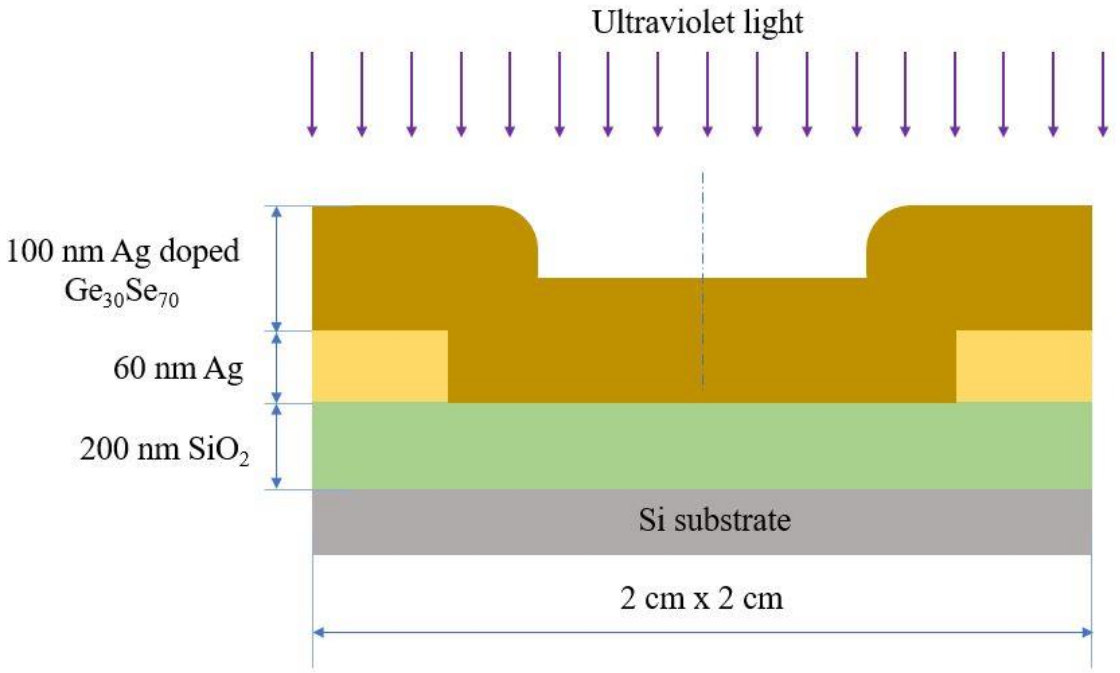

Figure 15: Photodissolution of Ag into $Ge_{30}Se_{70}$

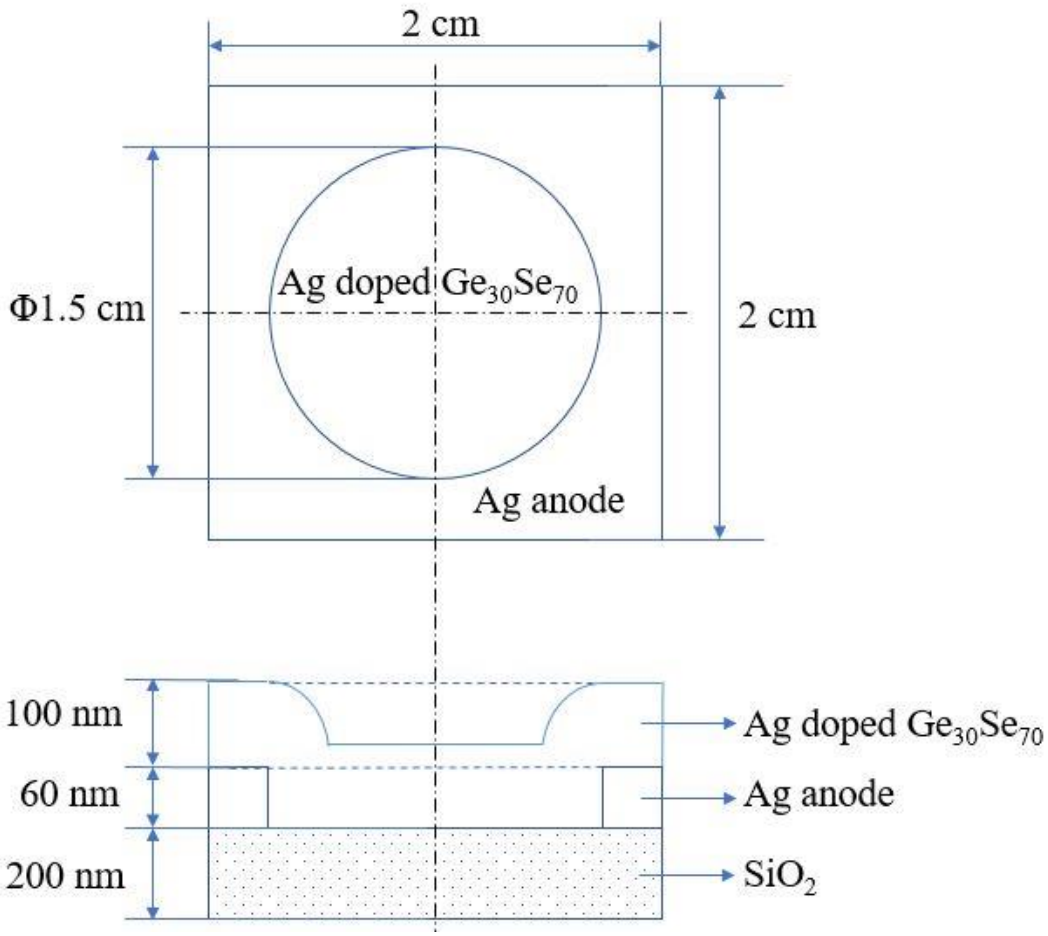

Figure 16: Structure of as fabricated radial PMC

5.1.5 Growth of electrodeposits

The electrodeposits were grown on the radial PMCs by biasing them with Agilent 4155C semiconductor parameter analyzer. The semiconductor parameter analyzer is able to apply voltage and measure current simultaneously. The devices were biased in a probe station which was also fitted with a hot temperature chuck. For the sake of simplicity, the devices fabricated in this work did not have a dedicated cathode, instead the W probe on the probe station was used as a cathode as shown in Fig. 17.

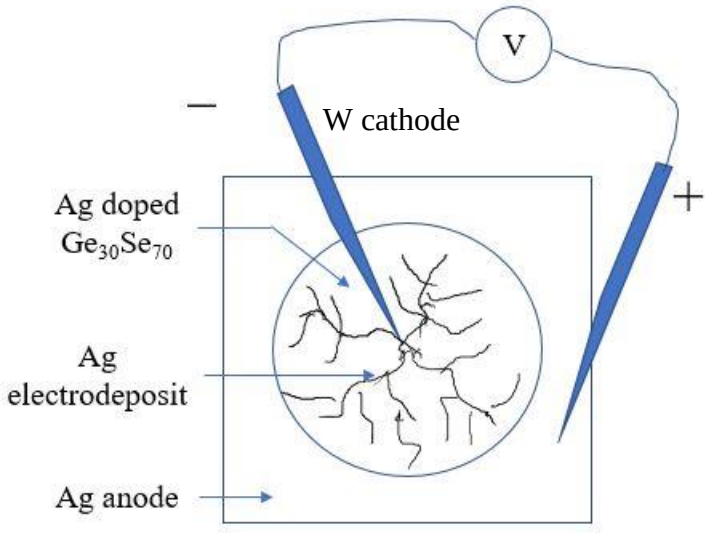

Figure 17: Growth of Ag electrodeposit

Extreme care was taken to probe the device at the center of the circular electrolyte region. The size of the electrodeposit is controlled by the time the electrochemical reaction is allowed to proceed by biasing the device. Electrodeposits were grown at different voltages and temperatures; the results will be discussed in upcoming section. Fig. 18 shows a picture of a dendrite taken from a tabletop camera.

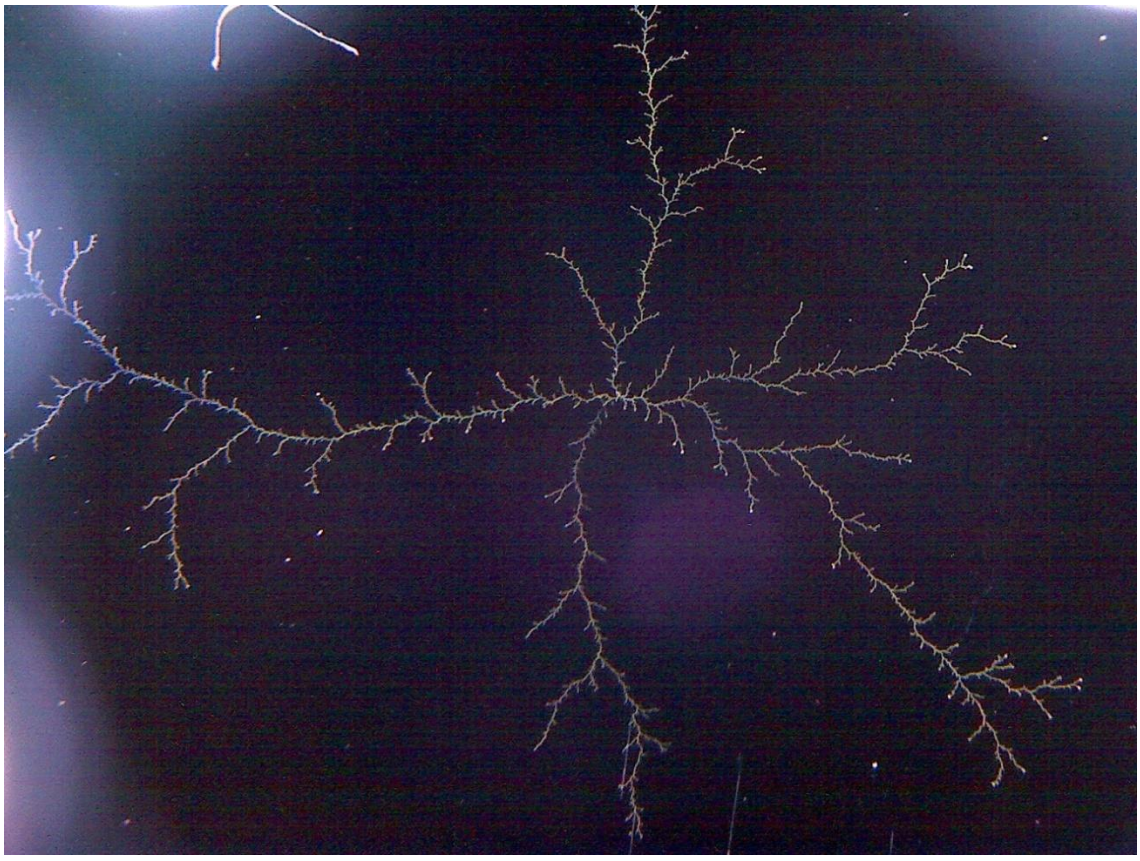

Figure 18: Tabletop camera image of Ag electrodeposit grown in radial PMC

5.2 Investigation of kinetics in the cell

5.2.1 High temperature growth in PMCs

It is important to investigate the basic processes in the growth of electrodeposits for a variety of reasons. A sound understanding of limiting processes in the radial PMCs is crucial to improve growth time, develop new materials, or even design new applications. To study the kinetics of the reactions, electrodeposits were grown in radial PMCs at different temperatures. The devices were fabricated as mentioned in earlier sections. The PMCs were biased in a probe station fitted with a hot chuck at 300 K, 325 K, 350 K, 375 K and 425 K. The electrodeposits were grown at 40 V constant bias for 200 s and current

through the cell was measured using Agilent 4155C semiconductor parameter analyzer. The current vs time (I-t) data at different temperatures from the growth of electrodeposits is shown in Fig. 19.

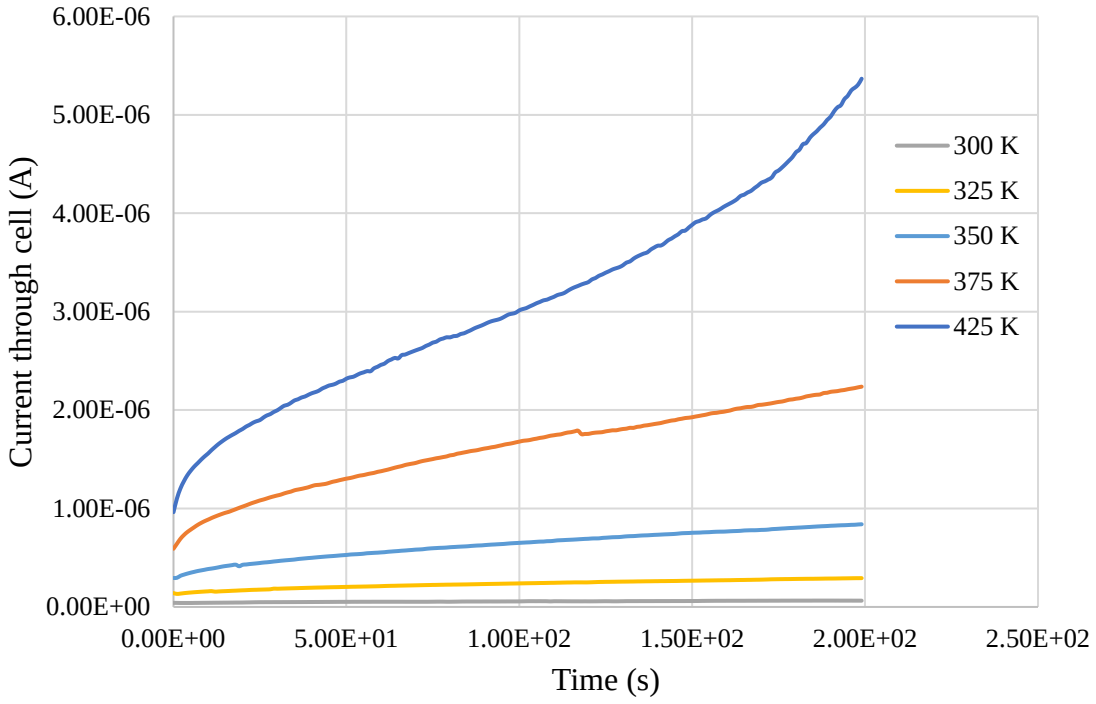

Figure 19: I-t curves for electrodeposit growth at high temperatures

It is reasonable to assume that the non-faradaic currents are negligible compared to the faradaic current since the anodic overpotential is extremely high (40V-E_{eq}) resulting in high reaction current. Moreover, the high overpotential also means that the activation energy for the redox reaction is probably very low (from Butler Volmer equation). Fig. 19 clearly shows that the current through the cell is a strong function of temperature. Moreover, the current in the cell increases with time and this increase in current is significant in electrodeposits grown at higher temperatures. This behavior of reaction

current signifies that the reaction in the cell has not reached a steady state even after 200s of reaction time. A probable explanation of this phenomenon is continuously increasing electric fields in the cell. As the reaction proceeds, the growing electrodeposit constantly shortens the distance between the circular anode and itself, therefore increasing the electric field under which the ions drift towards the metallic electrodeposit. The higher electric fields increase the flux of ions that feeds the growth which in turn accelerates the redox reaction and grows the electrodeposit further. This positive feedback effect is stronger at high temperatures owing to faster redox and transport processes compounding the effect even more, thus the non-steady state nature of the reaction.

To further investigate the dependence of current through the cell on temperature, an Arrhenius plot for the current value at 50 s was plotted as shown in Fig. 20. The current value at 50 s was chosen to avoid enhancement of electric field with time due to growth of electrodeposit as discussed earlier. Earlier than 50 s would also be disadvantageous because the non-faradaic currents in the system such as polarization current would have confounded the actual current values.

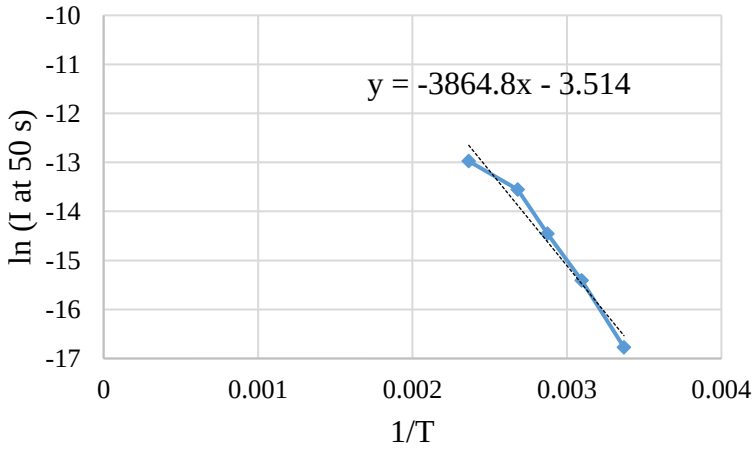

Figure 20: Arrhenius plot for current through the cell at 50 s

The plot deviates from linearity at 425 K. This can be attributed to degradation of film at high temperature as Ag doped $Ge_{30}Se_{70}$ loses stability above 120°C (395 K). However, current through the cell does indeed show Arrhenius behavior at lower temperatures, as can be seen from the figure. Therefore, the expression for the redox current in the cell may be written in the form,

$$I = I_0 exp\left(\frac{-E_a}{kT}\right). \quad 18$$

Where,

I = Current through the cell at temperature T,

I_0 = Pre-exponential factor,

E_a = Activation energy of the process,

k = Boltzmann constant, and

T = Absolute temperature.

The activation energy calculated from the fitting of line to the Arrhenius plot is 0.33 eV. It is important to note that the fitting of data with the Arrhenius type equation only signifies that the current through the cell is thermally activated with an activation energy

of 0.33 eV. Moreover, the calculated activation energy does not necessarily relate to the redox reactions or ionic transport for that matter, it is merely the activation energy of the limiting process in the cell. The rate limiting process will further be investigated in upcoming section.

The fact that the observed current through the cell is faradaic current allows us to get more information about the quantity of Ag that has been deposited by calculating the amount of charge exchanged through redox reactions. The area under the curve of I-t plot in Fig. 19 is the amount of charge transferred during the redox reactions for deposition of Ag. The amount of Ag deposited M in moles can be easily calculated from the redox charge Q by,

$$M = \frac{Q}{nF}. \qquad 19$$

Where,

M = Amount of Ag deposited in electrodeposits in moles,

Q = Charge exchanged during redox reaction,

n = Charge of Ag ion (1), and,

F = Faraday's constant.

Table 1: Amount of Ag deposited in electrodeposits at different temperatures

Absolute temperature (K)	Total exchanged charge (C)	# moles of Ag (mol)	Amount of Ag deposited (g)
300	1.11E-05	1.15E-10	1.24E-08
325	4.65E-05	4.82E-10	5.20E-08
350	1.26E-04	1.31E-09	1.41E-07
375	3.21E-04	3.32E-09	3.59E-07
425	6.21E-04	6.43E-09	6.94E-07

Table 1 shows the total redox charge, the amount of Ag deposited in electrodeposits in moles and grams. The deposited Ag increased by more than an order of magnitude from room temperature to 425 K. It is interesting to see that the amount of Ag photodissolved into the $Ge_{30}Se_{70}$ matrix (8.39×10^{-5} g, calculated from the volume of the film) to create the solid electrolyte, is three orders of magnitude more than the amount of Ag electrodeposited at room temperature. Since the amount of Ag needed to form the electrodeposit is so small compared to the amount of Ag in the solid electrolyte, one could argue that Ag anode is not needed for the reduction of Ag^+ ions at the cathode and subsequent growth of electrodeposit. However, without the Ag anode, there will not be an Ag oxidation reaction at the anode, which would defy charge neutrality and the reaction would not proceed. The function of Ag anode is to provide a counter reaction to the reduction of Ag^+ ions at cathode rather than to supply Ag^+ ions for the growth of electrodeposit. Moreover, the anode also acts as a contact to complete the electrical circuit. The electrodeposits could still be potentially grown without the fabricated Ag built into the structure, as long as there is an external Ag anode that could seamlessly oxidize by

dissolving into the solid electrolyte and provide a counter reaction to the reduction of Ag^+ into Ag at cathode.

5.2.2 Low temperature transport in Ag-$Ge_{30}Se_{70}$ solid electrolyte films

The high temperature growth experiment discussed in earlier section provided some insight into the rate limiting process during the growth of electrodeposits in radial PMCs. However, the response of the cell was confounded because of charge transfer reactions as well as drift-diffusive transport of ions from anode to cathode. The presence of electrodes that participated in the redox reactions made separation of the two processes from each other impossible. One could speculate that the redox reactions were not the rate limiting processes because of the high anodic overpotential but this claim needs to be corroborated with experimental findings. In this work, a new test structure was designed by utilizing blocking indium (In) electrodes to avoid any redox reactions at the electrode-electrolyte interface. The In does not take part in any known redox reactions with the materials involved and can be used to isolate ionic transport in the films.

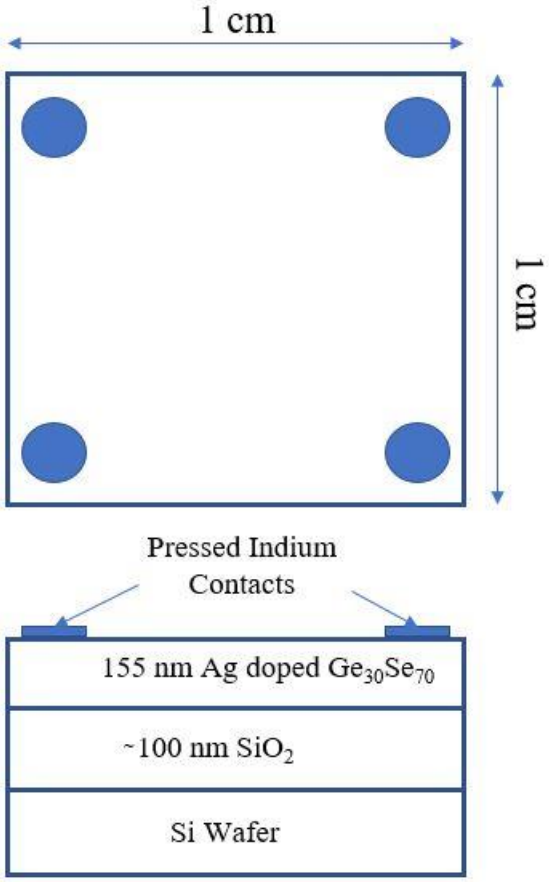

Figure 21: Schematic of the test structure used for low temperature characterization of the solid electrolyte.

The test structure was essentially a solid electrolyte with In contacts. Fig. 21 shows schematic of the test structure. It was fabricated at Nanoionic Prototyping Facility in Center for Applied Nanoionics at Arizona State University. The test structure was formed on oxidized Si wafer pieces diced into 1 cm x 1 cm squares. The thickness of the SiO_2 layer was about 100 nm. A 120 nm thick blanket film of $Ge_{30}Se_{70}$ was deposited on the diced and cleaned wafer pieces in Cressington 308R system. The chamber vacuum for deposition was better than $1x10^{-5}$ mbar, evaporation of $Ge_{30}Se_{70}$ was done by heating a boat containing

a glassy $Ge_{30}Se_{70}$ precursor at 4 V operating voltage and 35 A deposition current. The deposition rate was about 0.1 nm s^{-1} as monitored by crystal thickness monitor. Followed by the deposition of $Ge_{30}Se_{70}$, a 35 nm Ag blanket film which serves as a source of Ag for photodissolution in $Ge_{30}Se_{70,}$ was deposited without breaking the vacuum. The chamber vacuum for deposition was better than $1x10^{-5}$ mbar, evaporation of Ag was done by heating another boat containing Ag pellets at 4 V operating voltage and 45 A deposition current. The deposition rate was about 0.1 nm s^{-1} as monitored by crystal thickness monitor. The samples so prepared were irradiated with UV light for 2 hr to bring about photodissolution of Ag into the chalcogenide film. The UV light was UVA with 3.4 eV energy, the source had intensity of 3.5 mW cm^{-2}. Contacts were then formed at the four edges of the 1 cm x 1 cm solid electrolyte films by pressing indium contacts. The films were packaged by wire bonding the four In contacts.

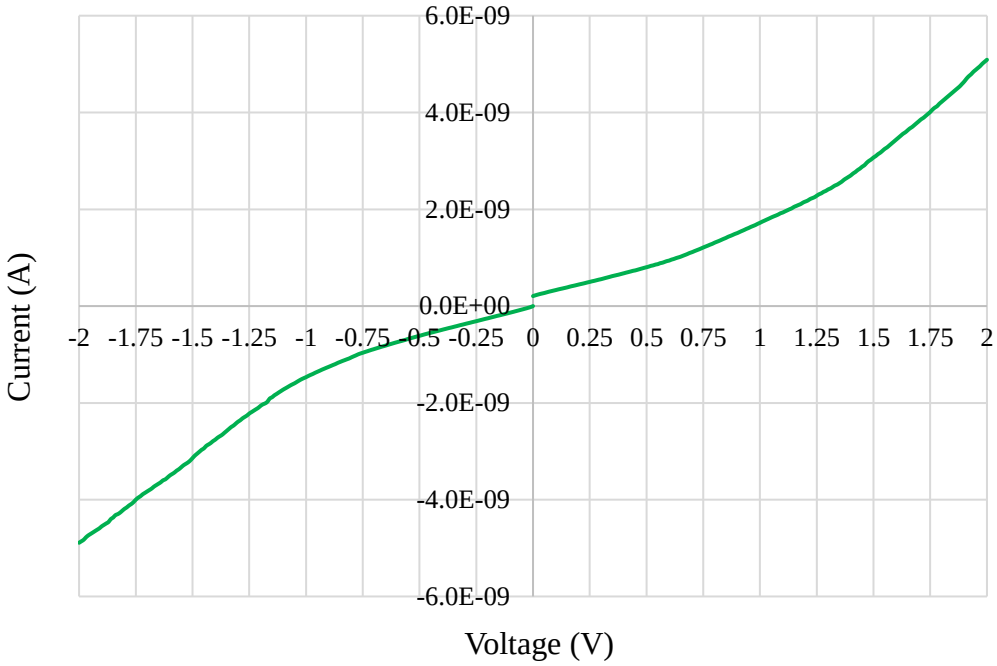

Figure 22: Typical I-V curve for current through the solid electrolyte film

The electrical response of the test structure was then evaluated at different low temperatures in the Newman Labs Facility at Arizona State University. The packaged films were mounted on a test probe and the test probe was dipped in helium (He) dewar. The temperature of the films can be varied by changing the height of the test probe in the dewar. The temperature was recorded with a thermocouple attached to the probe. The electrical response of the film was recorded between room temperature and 175 K in 25 K intervals using a HP 4140B. The film was biased between two adjacent contacts and the voltage was swept from 0 V to 2V followed by a voltage sweep from 0 V to -2 V at each temperature interval. It was found that the magnitude of current in positive and negative sweep was equal, confirming that the In contacts were essentially non-rectifying. Fig. 22 shows a typical current vs voltage (I-V) curve obtained from the sweeps. To evaluate the transport

properties of the solid electrolyte, the I-V behavior was fitted to high field model of Mott-Gurney transport, rewritten here from Eq. (7) for convenience.

$$j_{hop} = ZqN_i a\nu \exp\left(-\frac{W}{kT}\right)\exp\left(\frac{aZq\varepsilon}{2kT}\right), \quad 20$$

where,

a = Mean ionic hopping distance,

ν = Hopping frequency,

Zq = Charge on the cation,

N_i = Cation concentration,

T = Temperature (K),

K = Boltzmann constant,

W = Height of energy barrier and

ε = Applied electric field.

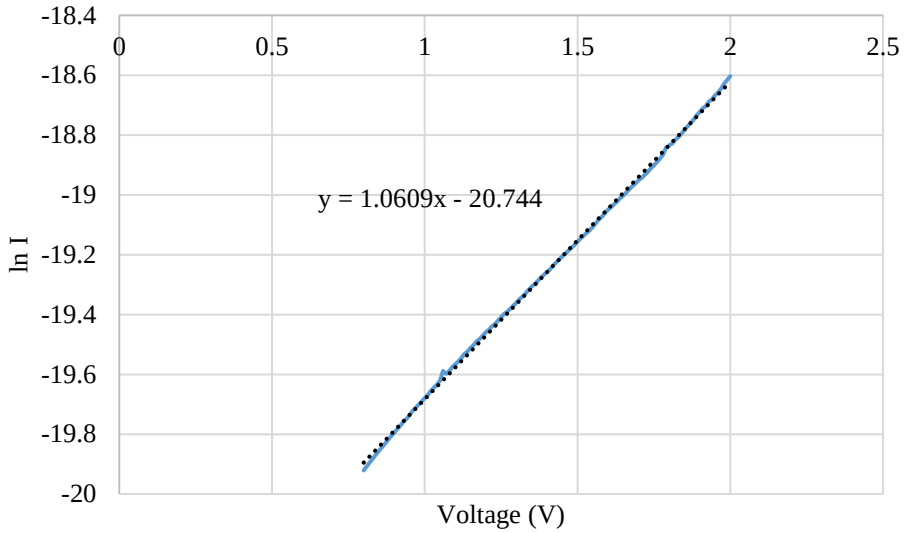

Figure 23: Ln I vs V plot for fitting of high field Mott-Gurney model

Fig. 23 shows the ln I vs V plot for the fitting high field Mott-Gurney model between 0.8 to 2 V. The voltage range of 0.8 to 2 V was chosen to ensure that the film was under high electric field. As can be seen from the plot, the I-V characteristics fit the high field Mott-Gurney model perfectly. By evaluating Eq. 20, for a thickness *d* of the film, the slope of the ln I vs V plot is,

$$slope = \frac{aZq}{2dkT}. \qquad 21$$

For 155 nm thickness of the solid electrolyte film in this study, the calculated hopping distance was 8.45 nm. The value of *a* is slightly larger than a typical ionic hopping distance value found in literature [9]. The distance may be attributed to the average distance the ions need to hop between two superionic phases in the Ge rich matrix.

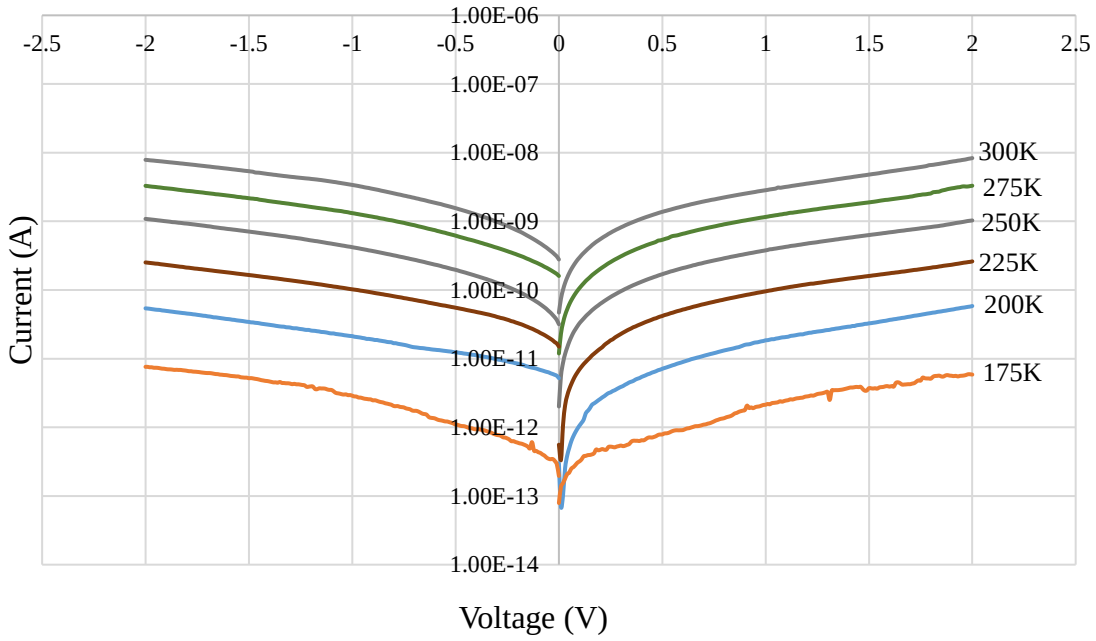

Figure 24: Low temperature I-V curves for temperatures between 300 K and 175 K

The results from low temperature I-V measurements are shown in Fig. 23. Clearly, the current through the test structure is a strong function of temperature. The initial current in negative voltage sweep is significantly larger than the corresponding current in positive voltage sweep, but the magnitudes of currents equalize at about 0.5 V and stay equal throughout the voltage range. This discrepancy may be attributed to non-faradaic currents during negative sweep or instrumental artifact. To further investigate the dependence of current through the test structure on temperature, an Arrhenius plot for the current values at 1 V, 1.5 V and 2 V was plotted as shown in Fig. 25. The current through the test structure shows Arrhenius behavior as can be seen from the figure. Therefore, the expression for the ionic transport current in the test structure may be written in the form of Eq. 18. The calculated activation energy Ea for the rate limiting process for transport of ions through the solid electrolyte is 0.259 eV, 0.257 eV and 0.259 eV at 1 V, 1.5 V and 2 V respectively.

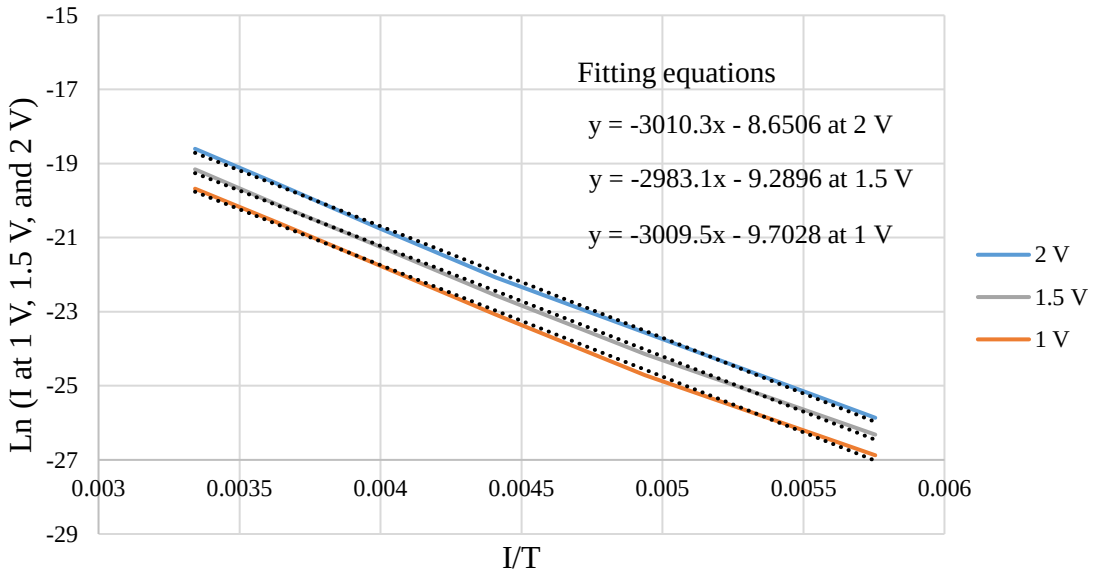

Figure 25: Arrhenius plot for current through the solid electrolyte film at 1 V, 1.5 V and 2 V, corresponding activation energies are 0.259, 0.257 and 0.259 eV

The calculated activation energy for transport of ions in solid electrolyte remains fairly constant at about 0.26 eV for different voltages. This value is clearly less than the activation energy of the rate limiting process in electrodeposit growth (0.33 eV) obtained from high temperature results in previous section. The Arrhenius dependence was studied further by fitting the data to high field Mott-Gurney transport model. The high field model of Mott-Gurney transport also shows Arrhenius dependence on temperature. By evaluating Eq. 20, for given thickness of the solid electrolyte film *d*, the slope of the Arrhenius plot for high field model of Mott-Gurney transport is given by,

$$slope = \frac{aZqV}{2kd} - \frac{W}{k}. \qquad 22$$

By substituting hopping distance a as 8.45 nm as calculated earlier, thickness *d* as 155 nm, and voltage V as 2 V, the energy barrier height W for ionic hopping was calculated to be

0.31 eV which shows excellent correlation with the energy barrier height values in the literature. The barrier height is also very close to the observed activation energy (0.33 eV) of rate limiting process in growth of electrodeposits.

The reduction of barrier height from 0.31 eV to 0.26 eV observed in the Arrhenius plot for ionic conduction through the solid electrolytes highlights a very important phenomenon in Mott-Gurney ionic transport. Under high electric fields, the barrier height for the potential well is reduced by ($aZq\varepsilon/2$) as can be seen in Eq. 7. The seemingly smaller activation energy of 0.26 eV in ionic transport compared to 0.33 eV in electrodeposit growth is a result of high electric fields in the solid electrolyte film owing to the blocking electrodes and smaller thickness. In case of growth in PMCs however, the reactive nature of electrodes causes the majority of the potential to drop at the electrode-electrolyte interface to bring about the redox reaction and consequently the electric field in the device is small. At smaller electric fields the Mott-Gurney model reduces to Eq. 8 and the barrier height is independent of the electric field. Nevertheless, the barrier height for hopping observed in low temperature ionic transport experiment is still smaller than the activation energy barrier during growth at high temperature, albeit by a very little extent. This can be attributed to the process variation and different concentration of Ag doped into the film; the amount of Ag photodoped into $Ge_{30}Se_{70}$ was deliberately kept lower to avoid presence of remnant Ag on top after photodissolution which could potentially act as nucleation center for electrodeposit growth.

From the above experiments, it is fair to say that the growth of electrodeposits in radial PMCs is limited by the mass transport owing to high overpotential which essentially

ensures the growth is not charge transport limited. It is important to note that, this is only true for radial PMCs which operate at high voltages and bigger distances between electrodes. This might not be the case in other PMCs. In vertical PMCs for example the operating voltage is very low to keep up with low power requirement of memory. At the same time, vertical PMCs are extremely thin. This might result in a condition that is exactly opposite to radial PMCs. The extremely high fields in vertical PMCs would mean the barrier for hopping will be lowered to very small value while the low operating voltage would mean there is very little overpotential for redox reaction, resulting in a charge transport limited process.

5.3 Materials characterization of electrodeposits

The metallic Ag electrodeposits grown at room temperature and high temperature were further studied with materials characterization techniques such as scanning electron microscopy (SEM), electron probe micro-analysis (EPMA) and atomic force microscopy (AFM). SEM was conducted at Center for Solid State Electronics Research, EPMA and AFM was performed at LeRoy Eyring Center for Solid State Science in Arizona State University.

SEM micrographs were taken using Hitachi S-4700 field emission scanning electron microscope. Fig. 26 and Fig. 27 show micrographs taken at 45000X magnification of a room temperature grown Ag electrodeposit and an electrodeposit grown at 375 K. Clearly, the treelike branching structure of the electrodeposit is still preserved at 45000X. This emphasizes the high information capacity potential of these fractal electrodeposits provided they can be analyzed. Both the images show grains of the electrolyte films and

the Ag electrodeposit. The high temperature grown electrodeposit shows coarsening of the grains in the electrolyte film as well as the electrodeposit. This coarsening may be attributed to the annealing effect experienced in the film grown at high temperature.

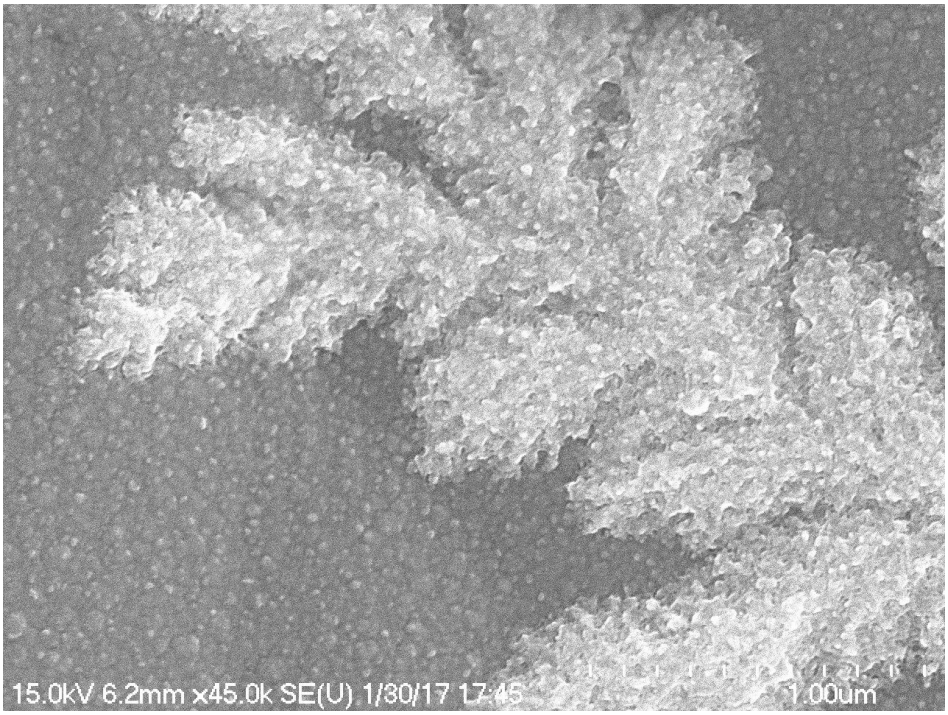

Figure 26: SEM micrograph of electrodeposit grown at room temperature

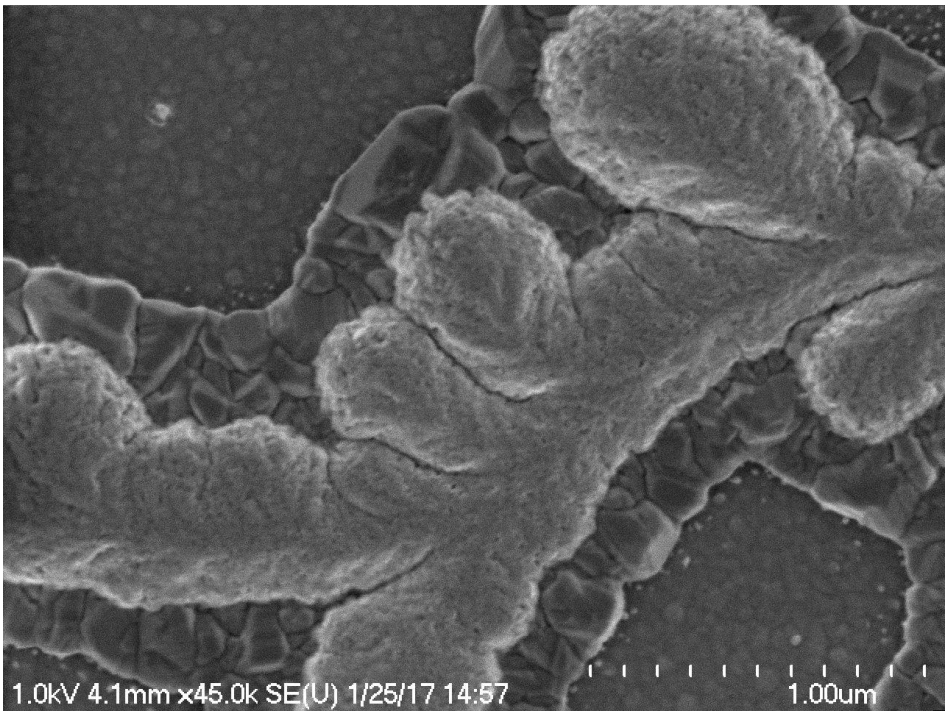

Figure 27: SEM micrograph of electrodeposit grown at 375 K

The most striking difference between the high temperature grown and room temperature grown electrodeposits is a new phase that forms a ‘collar’ around the electrodeposit in high temperature growth. It can be speculated that the new phase was formed as a result of annealing effect in the PMC. The high temperature grown electrodeposit was further analyzed by EPMA.

EPMA was performed on the electrodeposit by using JXA-8530F electron probe microanalyzer by JEOL. Fig. 28 shows results from EPMA on high temperature grown Ag electrodeposit.

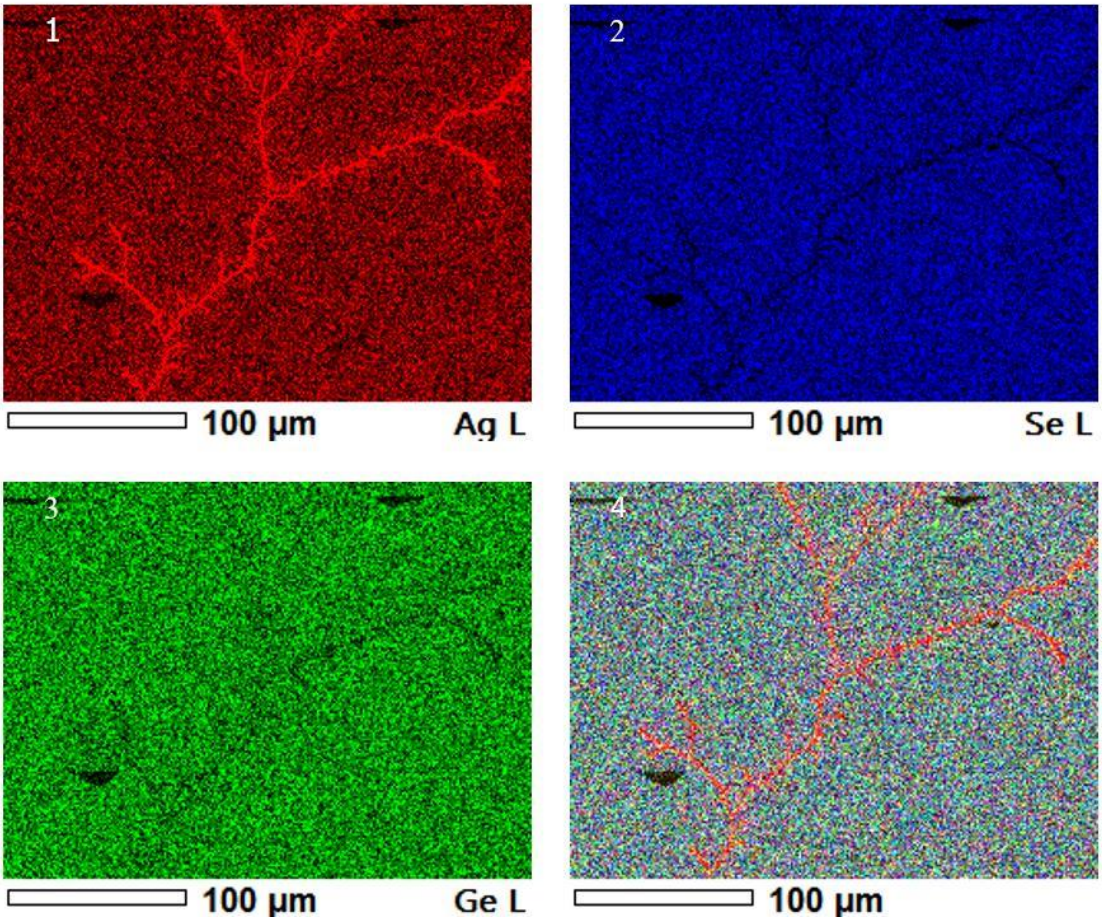

Figure 28: EPMA analysis results of electrodeposit grown at 375 K

Panel 1 shows signal from Ag L line in red, panel 2 shows signal from Se L line in blue, panel 3 shows signal from Ge L line in green and panel 4 is composite of images from panel 1 to 3. The electron beam currents used in EPMA are about 10 times higher than the beam currents in SEM, which causes the solid electrolyte film to exfoliate because of the heat generated from beam-material interaction. The black spotting at the bottom left and top right corner of the images is from exfoliation of the beam sensitive solid electrolyte. Moreover, the image was taken only at 400X because the problem exacerbated at higher magnification from severe localized heating. Therefore, elemental analysis of the high temperature phase was not possible.

Based on the available literature and the experimental results a potential explanation of the origin of high temperature phase is offered. Mitkova et al. [21] had observed that, upon thermal annealing of test structures containing Ag and $Ge_{20}Se_{80}$, the films undergo phase transformation and Ag_2Se phase is crystallized owing to the Ag-Se reaction being more energetically favorable than Ge-Se reaction. The high temperature of growth may have offered the energy needed for crystallization of Ag_2Se. Moreover, on closer examination of the EPMA in panels 1, 2 and 3, it can be seen that there is noticeable decrease in Se content of the film in the area where electrodeposit is grown while the Ge content is less affected by the Ag electrodeposit. This might be due to depletion of Se owing to formation of new phase. Even though it is tempting to suggest that the high temperature phase forming a collar around the electrodeposit is likely to be Ag_2Se, clearly further analysis is required to arrive at an incontestable conclusion.

The surface of the film and the electrodeposits was characterized by using AFM. A Bruker MultiMode 8 system was used to perform AFM on the samples. Fig. 29 shows the results from the areal scan of AFM. The scanned area was 80 µm x 80 µm. The AFM emphasizes the intricate surface features of the electrodeposit as can be seen from Fig. 29. Moreover, the bifurcation of branches can also be seen within an electrodeposit arm. The subtle branching within a major arm goes to show the inherent fractal nature of the electrodeposition process in PMCs.

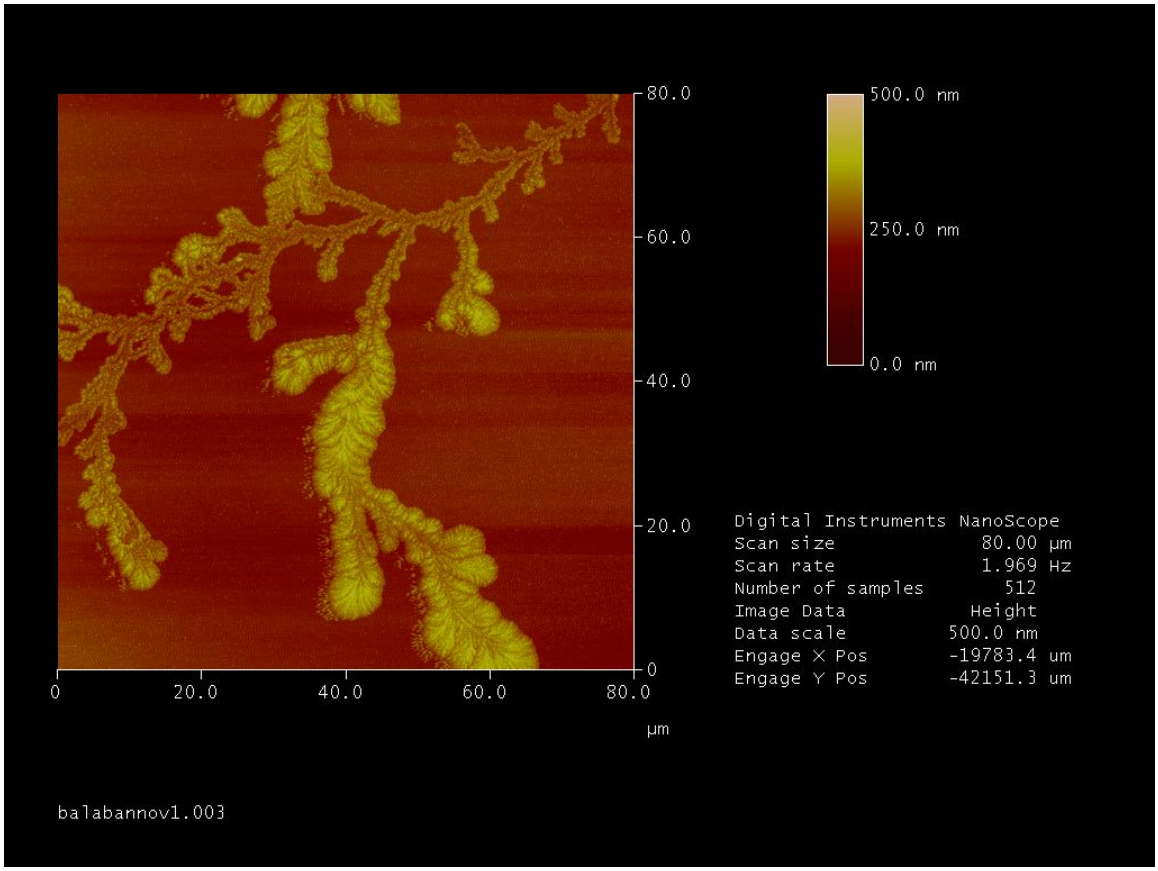

Figure 29: Areal scan of Ag electrodeposit using AFM

Fig. 30 shows the results from section analysis of an electrodeposit arm using AFM. The height of the electrodeposit ranges between 10s of nanometers to about 100 nm. The nanoscale features of the surface are evident from the figure. The surface morphology of the electrodeposit grants it some interesting optical properties which will be discussed in the next section.

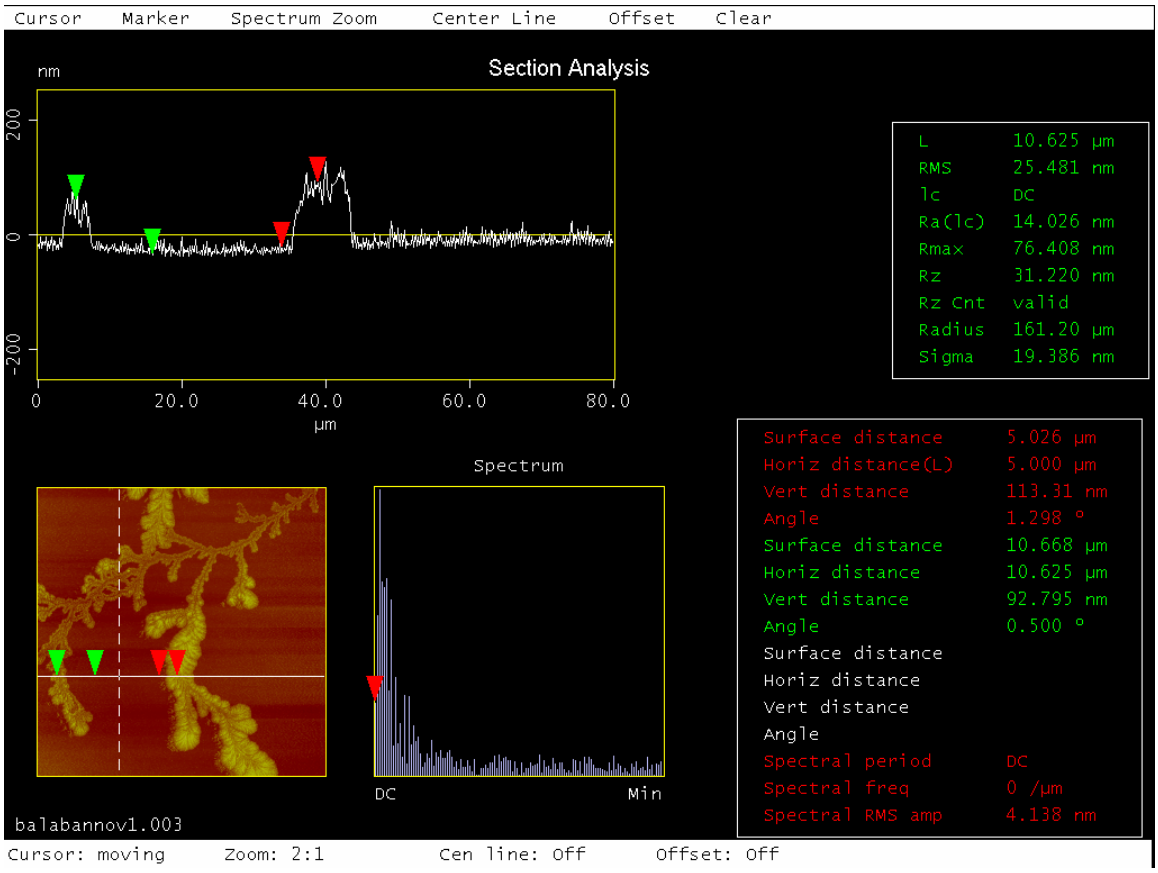

Figure 30: Section analysis of electrodeposit using AFM

5.4 Optical characterization of electrodeposits

The performance metric of electrodeposits for PUF application is their fractal dimension. Moreover, as was discussed in chapter 4, the use of Ag electrodeposits as PUF has a strong dependence on the scale at which its image is captured. Both quantities mentioned above relate to imaging of the electrodeposit, therefore it is vital to study the electrodeposits optically.

Fig. 31 shows a photomicrograph of an Ag electrodeposit taken at 100X using conventional bright-field microscopy technique. In bright-field microscopy, the transmitted sample illumination is collected by the objective lens and observed through the eyepiece. Fig 31 shows the brightness of the electrodeposit varies from one spot to other, some parts of the electrodeposit are hard to observe due to the brightness of the electrodeposit and the background being very similar to each other. Since the images of electrodeposits will be analyzed numerically, the lack of sufficient contrast between the electrodeposit and the background could potentially make accurate analysis of the image difficult.

Figure 31: Bright-field image of Ag electrodeposit at 100X

Fig. 32 shows image of the same electrodeposit at 100X using dark-field image of the same electrodeposit shown in Fig. 31. In dark-field imaging, the light used for illumination of the sample is not collected by the objective lens for creation of image. The optics are designed in such a way that only the scattered light from the sample enters the objective while directly transmitted light avoids it. Thus, dark-field images have a dark background with bright objects. The image shows better contrast between the electrodeposit and the background. However, some branches that could be well observed in bright-field image appear to have lost detail. A simple solution to this problem could be to use both bright-

field and dark-field technique to scan the electrodeposit and then use numerical techniques to form a composite image that combines details from both the techniques.

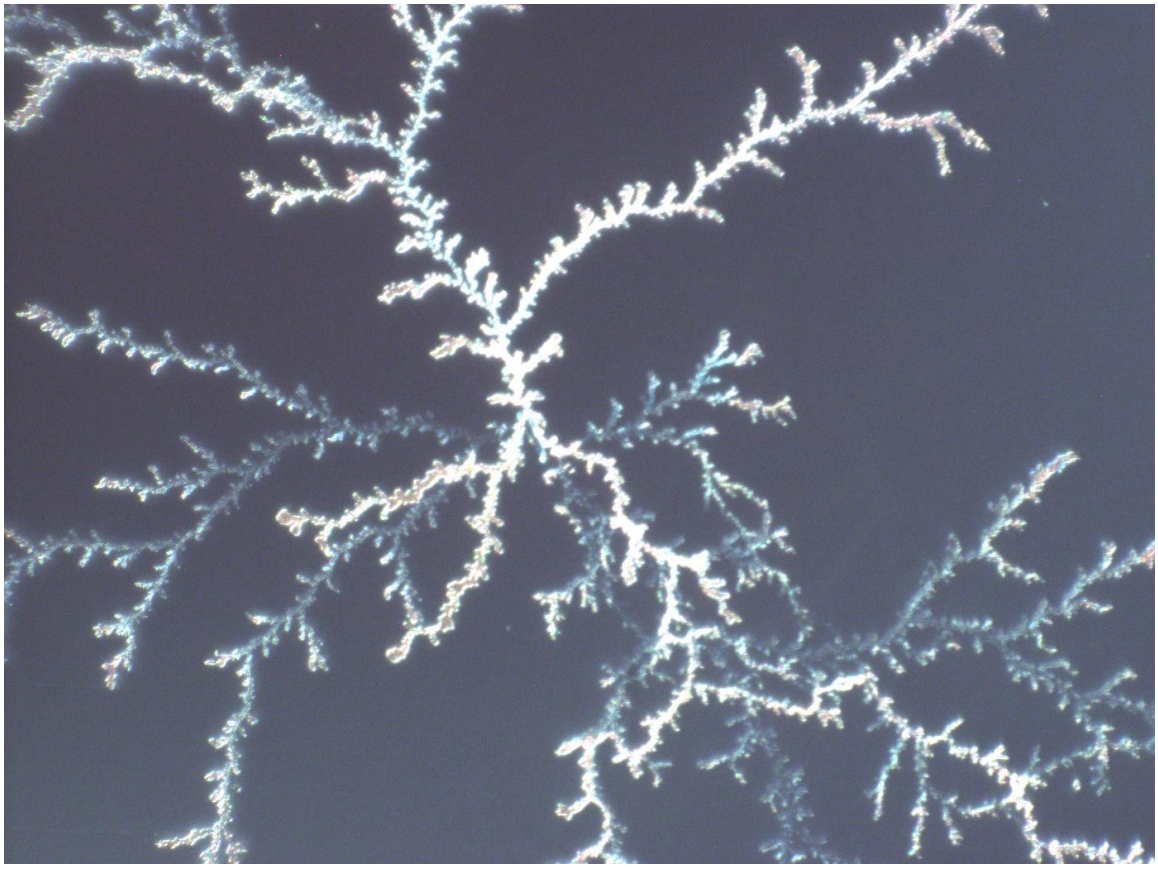

Figure 32: Dark-field image of Ag electrodeposit at 100X

The electrodeposit surface is unique in that it has a nanoscale subtle relief structure originating from the growth processes as was observed using AFM. The surface morphology of the electrodeposit is easy to observe but extremely difficult to copy. Therefore, it can be used as an added layer of protection in detecting counterfeit electrodeposit tags. The differential interference contrast (DIC) also known as Nomarski technique may be used to observe the electrodeposits optically as a go/no go test to determine if the electrodeposits are genuine. The DIC technique uses the principles of

interferometry to bring out otherwise invisible features in the sample by using optical path length information [22]. Fig. 33 shows path of light through a DIC microscope. The unpolarized light enters the first polarizing filter and leaves it as a plane polarized light at 45°. The Nomarski prism splits it into two separate polarized rays at 90° to each other. These two rays are then focused by the condenser lens to pass through the sample. The condenser lens focuses them such that they interact with two adjacent points on the sample separated by a small distance.

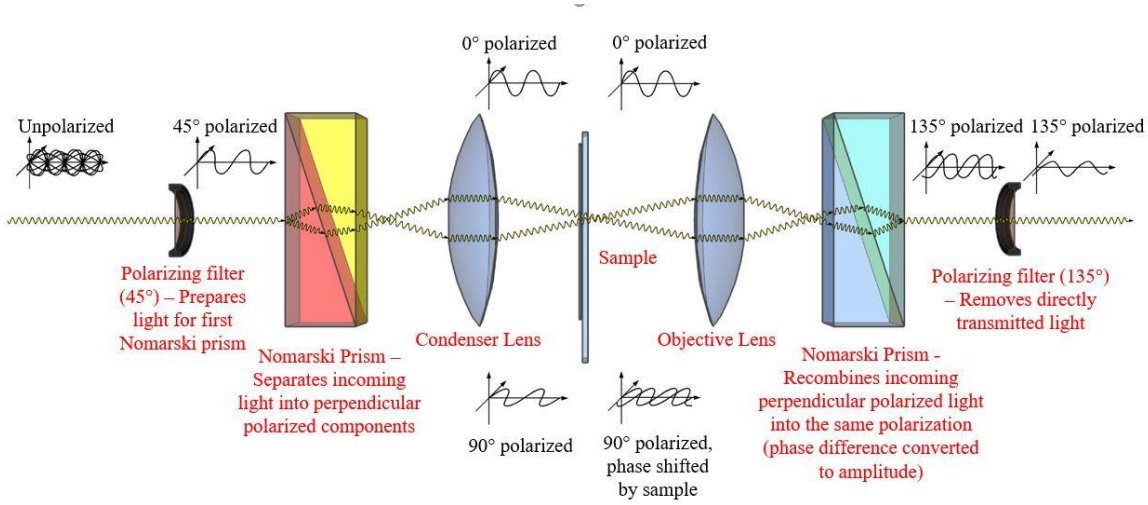

Figure 33: Path of light through a DIC microscope. Reprinted with permission from Richard Wheeler (en.wikipedia.org/wiki/User:Zephyris).

The two rays undergo change in their path length and consequently their phase if the two points on the sample differ in thickness or refractive index. The objective lens focuses these rays in the Nomarski prism which recombines the incoming perpendicular polarized light rays into one ray polarized at 135°. The recombination leads to interference which brightens or darkens the image depending on the optical path difference. Thus, the resultant image emphasizes texture and edges of the sample but is not topographically accurate.

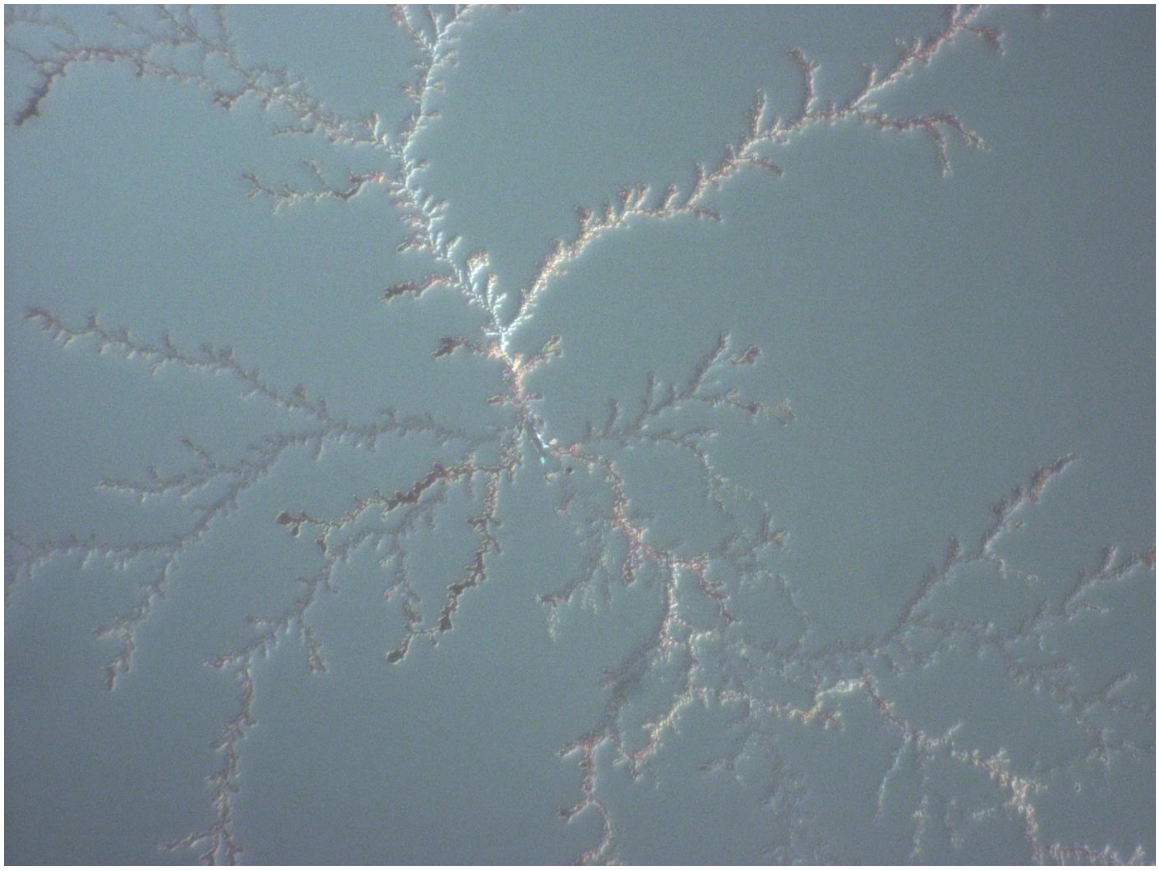

Figure 34: DIC image of Ag electrodeposit at 100X

Fig. 34 shows Nomarski DIC image of the same electrodeposit shown in Fig. 32 and 31 at 100X. It can be seen that the DIC technique emphasizes the morphology and 3rd dimensionality of the electrodeposit. Some branches of the electrodeposit may grow beneath the solid electrolyte film and others may grow on top of it. This uncertainty of growth may also be utilized to add another layer of security in the application of electrodeposits as secure tag. Thus, DIC technique is a simple and inexpensive alternative to AFM to verify the morphology and authenticity of the electrodeposit in PUF application.

6 CONCLUSION AND FUTURE WORK

In this thesis, fractal Ag electrodeposits grown in radial PMCs were investigated for their application as PUF. A simple recipe was developed for the fabrication of centimeter scale PMCs and macroscale electrodeposits were successfully grown. Fractal dimension of an electrodeposit was calculated by using box counting method and its information capacity was assessed. The fractal dimension of the electrodeposit was found to be 1.497 and its corresponding information capacity was calculated to be 1.27×10^{19}. Kinetics of growth process of the electrodeposits was assessed by electrical characterization of electrodeposit growth at high temperatures and electrical characterization of solid electrolyte by using blocking electrodes at low temperature. It was found that the growth process is mass transport limited, the Mott-Gurney ionic hopping being the rate limiting process. From fitting of the electrical data to the Mott-Gurney ionic hopping model, the average ionic hopping distance was found to be 8.45 nm and the energy barrier was found to be 0.31 eV. The electrodeposits grown at room and high temperature were characterized by using materials characterization techniques such as SEM, EPMA, AFM. A high temperature phase that forms a collar around the electrodeposit was discovered on analysis by SEM, further analysis by EPMA did not provide any conclusive results. The new phase is speculated to be Ag_2Se, however further analysis is required. AFM results revealed the 3-dimensional nature of the electrodeposit along with the formation of subtle branching within its arms during the growth. The electrodeposits were also characterized using optical techniques such as bright-field microscopy, dark-field microscopy and Nomarski DIC microscopy. It was observed that the combination of bright and dark-field images is the best approach to get the maximum information about the electrodeposit. Nomarski DIC

microscopy accentuated the topography of the surface of the electrodeposit hence proving itself to be a simple and inexpensive alternative to AFM for qualitative evaluation of the electrodeposit surface.

The enormous information capacity of the fractal electrodeposits, their simple fabrication with no complex processes, their easy to inspect but extremely difficult to replicate surface morphology, and their extremely high scalability make them a promising candidate for applications as PUFs in essentially all sectors.

However, much is yet to be learned about the electrodeposits and this thesis raises numerous questions. It befits this discussion to identify some of the opportunities for further investigation. The origin of randomness in the electrodeposit growth is still unknown. Since it was observed that the growth is mass transport limited, it could be speculated that the diffusive processes provide the randomness of the growth, but the effect of electric field and potential on the information entropy or perhaps fractal dimension is still very much unknown. Moreover, the Ag-chalcogenide materials system chosen in this work is not foundry friendly and is even frowned upon for being incompatible with materials used in microelectronics processing. The development of new foundry friendly materials for growth of fractal electrodeposits is another opportunity that has not been explored. Finally, new scanning and analysis strategies of the fractal electrodeposits for encoding and generating random numbers need to be formed to exploit their full potential.

REFERENCES

[1] M. N. Kozicki, M. Park, and M. Mitkova, “Nanoscale Memory Elements Based on Solid-State Electrolytes,” *IEEE Trans. Nanotechnol.*, vol. 4, no. 3, pp. 331–338, May 2005.

[2] M. N. Kozicki, “Dendritic structures and tags as physical unclonable function for anti-counterfeiting,” EP2998950 A1, 2016.

[3] W. Yu, “Fractal Properties and Applications of Dendritic Filaments in Programmable Metallization Cells,” 2015.

[4] M. N. Kozicki and W. C. West, “Programmable metallization cell structure and method of making same,” US5896312A, 1999.

[5] M. N. Kozicki, “Non-Volatile Timing Device,” 2015.

[6] J. A. Nessel, R. Q. Lee, C. H. Mueller, M. N. Kozicki, Minghan Ren, and J. Morse, “A novel nanoionics-based switch for microwave applications,” in *2008 IEEE MTT-S International Microwave Symposium Digest*, 2008, pp. 1051–1054.

[7] M. N. Kozicki, P. Maroufkhani, and M. Mitkova, “Valving in microchannels via electrodeposition on solid electrolytes,” vol. 1, pp. 716–719, 2005.

[8] I. Valov and M. N. Kozicki, “Cation-based resistance change memory,” *J. Phys. D. Appl. Phys.*, vol. 46, p. 74005, 2013.

[9] M. N. Kozicki and H. J. Barnaby, “Conductive bridging random access memory—materials, devices and applications,” *Semicond. Sci. Technol.*, vol. 31, no. 11, p. 113001, 2016.

[10] I. Valov, R. Waser, J. R. Jameson, and M. N. Kozicki, “Electrochemical metallization memories--fundamentals, applications, prospects.,” *Nanotechnology*, vol. 22, p. 254003, 2011.

[11] M. I. Mitkova, M. N. Kozicki, and J. P. Aberouette, “Morphology of electrochemically grown silver deposits on silver-saturated Ge-Se thin films,” *J. Non. Cryst. Solids*, vol. 326–327, pp. 425–429, 2003.

[12] M. Mitkova and M. N. Kozicki, “Ag-photodoping in Ge-chalcogenide amorphous thin films-Reaction products and their characterization,” *J. Phys. Chem. Solids*, vol. 68, no. 5–6, pp. 866–872, 2007.

[13] A. J. Bard and L. R. Faulkner, *Electrochemical Methods: Fundamentals and Applications*, 2nd ed. Wiley, 2000.

[14] N. Mott and R. W. Gurney, *Electronic Processes in Ionic Crystals*, 2nd ed. Clarendon Press, 1940.

[15] C. Herder, M.-D. Yu, F. Koushanfar, and S. Devadas, "Physical Unclonable Functions and Applications: A Tutorial," *Proc. IEEE*, vol. 102, no. 8, pp. 1126–1141, Aug. 2014.

[16] T. A. Witten and L. M. Sander, "Diffusion-Limited Aggregation, a Kinetic Critical Phenomenon," *Phys. Rev. Lett.*, vol. 47, no. 19, pp. 1400–1403, Nov. 1981.

[17] T. A. Witten and L. M. Sander, "Diffusion-limited aggregation," *Phys. Rev. B*, vol. 27, no. 9, pp. 5686–5697, 1983.

[18] Y. Sawada, A. Dougherty, and J. P. Gollub, "Dendritic and Fractal Patterns in Electrolytic Metal Deposits," *Phys. Rev. Lett.*, vol. 56, no. 12, pp. 1260–1263, Mar. 1986.

[19] B. B. Mandelbrot, *The Fractal Geometry of Nature*, 1st ed. W. H. Freeman and Company, 1982.

[20] P. S. Addison, *Fractals and Chaos: An illustrated course*, 0th ed. Institute of Physics Publishing, 1997.

[21] M. Mitkova, M. N. Kozicki, H. C. Kim, and T. L. Alford, "Local structure resulting from photo and thermal diffusion of Ag in Ge–Se thin films," *J. Non. Cryst. Solids*, vol. 338–340, no. 1 SPEC. ISS., pp. 552–556, Jun. 2004.

[22] M. G. Nomarski, "Interferential polarizing device for study of phase objects," 1960.